1521-009X/50/8/1098–1105$35.00
DRUG METABOLISM AND DISPOSITION

dx.doi.org/10.1124/dmd.122.000870
Drug Metab Dispos 50:1098–1105, August 2022

HepaRG Cells Adopt Zonal-Like Drug-Metabolizing Phenotypes under Physiologically Relevant Oxygen Tensions and Wnt/β-Catenin Signaling[S]

Thomas J. DiProspero, Lauren G. Brown, Trevor D. Fachko, and Matthew R. Lockett

Department of Chemistry, Kenan and Caudill Laboratories (T.J.D., L.G.B., T.D.F., M.R.L.), and Lineberger Comprehensive Cancer Center, School of Medicine (M.R.L.), University of North Carolina at Chapel Hill, Chapel Hill, North Carolina

Received February 13, 2022; accepted May 26, 2022

ABSTRACT

The cellular microenvironment plays an important role in liver zonation, the spatial distribution of metabolic tasks among hepatocytes lining the sinusoid. Standard tissue culture practices provide an excess of oxygen and a lack of signaling molecules typically found in the liver. We hypothesized that incorporating physiologically relevant environments would promote postdifferentiation patterning of hepatocytes and result in zonal-like characteristics. To test this hypothesis, we evaluated the transcriptional regulation and activity of drug-metabolizing enzymes in HepaRG cells exposed to three different oxygen tensions, in the presence or absence of Wnt/β-catenin signaling. The drug-metabolizing activity of cells exposed to representative periportal (11% O_2) or perivenous (5% O_2) oxygen tensions were significantly less than cells exposed to ambient oxygen. A comparison of cytochrome P450 (P450) 1A2, 2D6, and 3A4 activity at periportal and perivenous oxygen tensions showed significant increases at the lower oxygen tension. The activation of the Wnt/β-catenin pathway only modestly impacted P450 activity at perivenous oxygen tension, despite a significant increase in *P450* expression under this condition. Our results suggest oxygen tension is the major contributor to zonal patterning in HepaRG cells, with the Wnt/β-catenin signaling pathway playing a lesser albeit important role. Our datasets also highlight the importance of including activity-based assays, as transcript data alone do not provide an accurate picture of metabolic competence.

SIGNIFICANCE STATEMENT

This work investigates the postdifferentiation patterning of HepaRG cells cultured at physiologically relevant oxygen tensions, in the presence and absence of Wnt/β-catenin signaling. HepaRG cells exposed to periportal (11% O_2) or perivenous (5% O_2) oxygen tensions display zonation-like patterning of both cytochrome P450 and glucuronosyltransferase enzymes. These datasets also suggest that oxygen is a primary regulator of postdifferentiation patterning, with Wnt/β-catenin having a lesser effect on activity but a significant effect on transcriptional regulation of these enzymes.

Introduction

The primary human hepatocytes (PHHs) used in early assessments of hepatotoxicity often fail to predict the drug-induced liver injuries discovered during clinical trials (Kenna and Uetrecht, 2018; Parasrampuria et al., 2018). One reason for this failure is the ready dedifferentiation of PHHs under standard culture conditions. The collagen sandwich is an early example of how culture format could greatly improve the health, polarization, and metabolic activity of PHHs (Dunn et al., 1989; Dunn et al., 1992; Meyer et al., 2015). A continued and concerted effort to further improve PHH performance and predictability includes incorporating of three-dimensional tissue-like architectures (Usta et al., 2015; Shin et al., 2018; Kang et al., 2020), adding liver-specific soluble factors (Meyer et al., 2015), or replacing the PHHs with hepatocyte-derived cells lines or stem cells (Gerets et al., 2012; Bell et al., 2018).

Cues from the tissue microenvironment orchestrate liver-specific functions and zonation, the spatial and temporal distribution of metabolic tasks along each sinusoid (Oinonen and Lindros, 1998). Zonation is a result of postdifferentiation patterning (Jungermann and Kietzmann, 2000; Gebhardt and Matz-Soja, 2014), regulated by abiotic factors, such as oxygen and glucose, required to maintain cellular health and energy reserves. In the periportal (PP) region of the sinusoid, drug-rich blood enters from the portal triad and has an oxygen tension of 65–60 mm Hg or 11–8% O_2 (Kietzmann, 2017). Hepatocytes in this region carry out oxygen-intensive processes such as gluconeogenesis and urea synthesis (Braeuning et al., 2006). Blood exits the sinusoid through a central vein in the perivenous (PV) region and has an oxygen tension of 35–30 mm Hg or 5–3% O_2 (Kietzmann, 2017). Here, hepatocytes generate energy reserves through glycolysis and perform the majority of drug metabolism, including cytochrome P450 (P450)-mediated transformations (el Mouelhi and Kauffman, 1986; Braeuning et al., 2006).

Other zonation-regulating cues are morphogens and hormones, which modulate P450 expression through the activation of signaling pathways and nuclear receptors. Three pathways known to promote

This work was supported by the National Institutes of Health National Institute of General Medical Sciences [Grant R35-GM128697] (to M.R.L.).

A portion of this work was performed at the University of North Carolina's Department of Chemistry Mass Spectrometry Core Laboratory, which is funded in part by the Office of Research at University of North Carolina School of Medicine.

dx.doi.org/10.1124/dmd.122.000870.

[S] This article has supplemental material available at dmd.aspetjournals.org.

ABBREVIATIONS: AhR, aryl hydrocarbon receptor; HIF, hypoxia inducible factor; P450, cytochrome P450; PHH, primary human hepatocyte; PP, periportal; PV, perivenous; SULT, sulfotransferase; UGT, glucuronosyltransferase; WRN, Wnt3a, R-spondin 3, and noggin.

zonal phenotypes are the hypoxia-inducible factor (HIF) pathway, the Wnt/β-catenin pathway, and the hedgehog pathway (Giera et al., 2010; Matz-Soja et al., 2013; Kietzmann, 2019). HIF-regulated pathways are associated with transcriptional-level zonation patterns of phase I and II drug-metabolizing enzymes, urea synthesis, and albumin production. The stabilization of β-catenin facilitates the expression of glutamine synthase, a key enzyme in ammonia detoxification (Benhamouche et al., 2006; Gebhardt et al., 2007; Gerbal-Chaloin et al., 2014). A high concentration of Wnt is found in the perivenous region of the sinusoid, secreted by endothelial cells of the central vein (Gebhardt et al., 2007; Wild et al., 2020).

To date, in vitro studies of postdifferentiation patterning have focused on the role of oxygen or Wnt ligands individually. None to our knowledge have systematically evaluated the effect of both factors on the transcriptional regulation and activity of drug-metabolizing enzymes. Here, HepaRG cells maintained on collagen slabs were exposed to representative PP or PV oxygen tensions, in the presence and absence of Wnt/β-catenin signaling. We chose the HepaRG cell line because they have a high metabolic competency, are readily available, and eliminate experimental artifacts that can arise from donor-dependent PHH metabolic profiles. The HepaRG cell line also expresses phase II metabolic enzymes, including members of the glucuronosyltransferase (UGT) and sulfotransferase (SULT) families (Yokoyama et al., 2018). Previous studies showed that the HepaRG cell line could maintain a differentiated state and P450 activity for days to weeks in culture (Jackson et al., 2016).

Our results highlight that oxygen and the Wnt/β-catenin signaling pathway influence the activity and transcriptional regulation of P450s and phase II enzymes. When exposed to a representative PP (11% O_2) or PV (5% O_2) oxygen tension, there was a significant decrease in activity compared with standard culture conditions. A comparison of cells exposed to PV and PP oxygen tensions had enzyme activity and transcriptional regulation patterns that agree with zonation. The inclusion of Wnt3a, R-spondin 3, and noggin (WRN) signaling molecules at each oxygen tension highlighted the fact that changes in enzyme activity were dictated predominately by oxygen and further refined through the Wnt/β-catenin signaling pathway.

Materials and Methods

Chemicals. All chemicals and reagents were used as received unless otherwise specified. Chlorzoxazone, dextromethorphan (hydrobromide hydrate), (S)-mephenytoin, midazolam, testosterone, and acetaminophen-d_4 were purchased from Cayman Chemical Company. Collagen I (rat tail) was purchased from Enzo Life Sciences. Collagenase (*Clostridium histolyticum*), phenacetin, dextrorphan-d_3, bupropion hydrochloride, and sodium hydroxide (NaOH) were purchased from Millipore Sigma. DMSO and 7-hydroxycoumarin were purchased from Fisher Scientific. Hydroxybupropion-d_6 was purchased from Cambridge Isotope Laboratories. 6-hydroxychlorzoxazone-d_2 was purchased from Clearsynth. 7-hydroxycoumarin-d_5-sulfate and 7-hydroxycoumarin-$^{13}C_6$-glucuronide were purchased from Toronto Research Chemicals. 4-hydroxymephenytoin-d_3 was purchased from MuseChem. Hydroxymidazolam-$^{13}C_3$ and hydroxytestosterone-d_7 were purchased from Corning.

HepaRG Cell Culture. Differentiated NoSpin HepaRG Cryopreserved Cells were obtained from Lonza Bioscience. Before seeding cells into a 12-well plate, each well was coated with 500 μl of 2 mg/ml collagen I. The collagen suspension was neutralized with 1M NaOH and PBS, and the volume adjusted with reverse osmosis filtered water to a final concentration of 2 mg/ml. The collagen slabs were incubated overnight, washed with 1X PBS, and then seeded with HepaRG cells at a final density of 2.6×10^5 cells/cm^2.

All culture medium and supplements needed to maintain the HepaRG cells were obtained from Lonza. Unless otherwise noted, the cells were maintained at 37°C, 20% O_2, and 5% CO_2 in HepaRG medium containing a basal medium supplement, a maintenance and metabolism supplement, and 1% PenStrep. We refer to this medium composition as "Std Medium" throughout the text. Freshly thawed cells were plated in HepaRG medium containing a basal medium supplement, a thawing and plating supplement, and 1% PenStrep. After 24 hours, Std Medium was added and exchanged every 2 days. After 6 days, the HepaRG cells were exposed to either ambient oxygen tension, a representative PP tension (11% O_2), or a representative PV tension (5% O_2). These oxygen tensions were regulated with a custom-built hypoxia chamber, as detailed previously (DiProspero et al., 2021). Brightfield images of the HepaRG cells were captured on a Nikon TE2000 microscope, equipped with a 10X Plan Fluor objective (NA 0.3 WD) and Photometrics Dyno CCD camera.

LWRN Cell Culture and Secretion. The L- and L-WRN cell lines were purchased from the American Type Culture Collection and maintained as monolayers at 37°C, 20% O_2, and 5% CO_2 in Dulbecco's modified Eagle's medium supplemented with 10% FBS, 0.5 mg/ml G-418, and 0.5 mg/ml hygromycin B. Culture medium was exchanged every 2–3 days and the cells passed at 80% confluency with TrypLE, using standard procedures.

Conditioned medium was collected from both cell lines following the American Type Culture Collection–recommended protocol. Briefly, the cells were grown to confluency in a T150 flask without G-418 or hygromycin B. The cells were then washed with 1X PBS, 25 ml fresh medium was added, and the cells were collected after 24 hours. The conditioned medium was centrifuged at 1000 × g for 5 minutes, the supernatant decanted, and then stored at 4°C. Conditioned medium collected from 4 consecutive days was pooled, sterile filtered (0.22 μm), and stored at –80°C.

Evaluation of P450 Activity. Drug-metabolizing enzyme activity was quantified using a previously reported liquid chromatography-tandem mass spectrometry (LC-MS/MS) method (Dierks et al., 2001; Li et al., 2015). The HepaRG cells were washed with 1X PBS and incubated for 2 hours at 37°C in fresh Std Medium containing a cocktail of eight different enzyme substrates (Supplemental Table 1). Stock solutions of each substrate were prepared in DMSO at 1000× the working concentration and added to the HepaRG medium directly before use. The metabolite-containing medium was mixed with ice-cold acetonitrile (−20°C, Optima; Fisher Scientific) at a 1:10 (v/v) ratio to precipitate protein. Precipitated protein was removed with centrifugation (12,000 × g, 15 min), the supernatant was collected, and then protein was concentrated in vacuo. The residual solid was resuspended in 100 μl of high performance liquid chromatography-grade water (Optima).

Samples were separated on a Waters Acquity ultra performance liquid chromatography equipped with a BEH C18 column (2.1 × 50 mm, 1.7 μm) using a binary solvent system of 0.1% formic acid (v/v) in water (A) and 0.1% formic acid (v/v) in acetonitrile (B). The total run time of each separation was 9 minutes, using the following gradient profile at a 0.3-ml/min flow rate: 10% B for 1 minute; a linear gradient to 70% B over 5 minutes; 95% B for 1 minute; 10% B for 2 minutes to reequilibrate the column. Metabolites were quantified with selected reaction monitoring on a Thermo TSQ Vantage triple quadrupole mass spectrometer (MS). The MS source parameters were a heated electrospray ionization probe, 300°C; capillary temperature, 300°C; spray voltage, 4.8 kV; vaporization temperature, 300°C; sheath gas flow, 50; auxiliary gas flow, 15; S-lens RF amplitude, 120 V. Nitrogen was used for the sheath and auxiliary gases; argon was used as the collision gas. Two transitions of each product and internal standard were monitored, except for 4'-hydroxymephenytoin-d_3, where only a single transition could be monitored due to instrument limitations. The optimized declustering voltage and collision energies of each product and internal standard are listed in Supplemental Table 1. Data were collected and processed with the Xcalibur software package.

A substrate and product-free matrix control (culture medium containing basal supplement) was included in each run to ensure there were no coeluting interferents. A quality control sample, consisting of 10 μM each analyte, was analyzed after every 10 injections to monitor instrument drift. The analyte-to-internal standard ratio of each enzyme product was averaged across three separately prepared cell cultures. To assess changes in P450 activity, the analyte-to-internal standard ratios were normalized to a particular experimental condition. Using datasets obtained from consecutive injections of product standards (Supplemental Fig. 1), we determined a fold change of $1.25 > x > 0.8$ was not overlapping ($P < 0.0001$).

Urea Production. Before analysis, the cells were washed with 1X PBS and then incubated in fresh culture medium for 1 hour. The urea concentration was determined with the QuantiChrom Urea Assay Kit (BioAssay Systems), according to the manufacturer's protocol. Absorbance values (430 nm) were measured on a SpectraMax i3x Microplate Reader.

Transcript Expression Quantification. Prior to lysis, the cells were washed with 1X PBS. The RNA was collected and purified with a TRIzol Plus RNA purification kit (ThermoFisher), according to the manufacturer's protocol. Reverse transcription was performed immediately after RNA isolation with a High-Capacity cDNA Reverse Transcription Kit (ThermoFisher) in an Eppendorf Master Cycler. Amplification reactions for quantitative polymerase chain reaction were prepared in a 384-well plate with PowerUp SYBR Master Mix (ThermoFisher). Each gene was measured in triplicate on a QuantStudio 6 Flex Real-Time Polymerase Chain Reaction system using the following program: 95°C for 60 seconds, followed by 40 cycles of 95°C for 2 seconds and 60°C for 30 seconds. Supplemental Table 2 lists the primer sequences, optimal primer concentrations, and reaction efficiencies (90–110%) of each gene of interest. Each transcript was quantified using the ΔΔCt method against *18sRNA*. A fold change of greater than 2.0 was considered significant (USFDA, 2020).

Cell viability Measurements. The CellTiter-Glo reagent (CTG; Promega) was used to quantify cellular ATP levels, which we used as an indirect measurement of glucose metabolism. Before analysis, the cells were washed with 1X PBS and incubated at 25°C for 20 minutes in a 1:1 (v/v) solution of 1X PBS and the CTG reagent. Lysate aliquots (75 µl) were analyzed in an opaque 96-well plate on a SpectraMax i3x Microplate Reader, in luminescence mode with a 140-ms integration time. A tri-color live–dead stain of calcein AM, propidium iodide, and Hoechst 33364 was used to count the viable cells. Before staining, the cells were removed from the culture dish with a 15-minute incubation in 1 ml collagenase solution (1:10 w/v in TESCA buffer) at 37°C. The solution was triturated for 5 minutes before centrifugation at 1000 × g for 5 minutes. The cell pellet was resuspended in 1X PBS containing 2 µg/ml calcein-AM, 3 µg/ml propidium iodide, and 10 µg/ml Hoechst. After 10 minutes, the cells were pelleted and washed with 1X PBS. Cell aliquots were imaged on a Nikon TE2000 microscope equipped with a 10X Plan Fluor objective and a Photometrics Dyno CCD camera.

Statistical Analysis. All datasets are reported as the average and S.E.M. of measurement collected from at least four separately prepared cultures measurements, from at least two separate vials of cryopreserved HepaRG cells. All datasets were analyzed with GraphPad Prism 7. Statistically significant differences correspond to a *P* value of 0.05 or less, unless otherwise noted.

Results

Figure 1 summarizes the experimental approach used in this work. Differentiated HepaRG cells were plated on collagen slabs and exposed to one of nine different environmental conditions: combinations of three oxygen tensions and three medium compositions. This experimental design allowed us to quantify the effects of oxygen tension and Wnt/β-catenin signaling separately and in combination. The selected oxygen tensions were ambient conditions used in standard tissue culture practices (Std O_2), a representative periportal tension of 11% O_2 (PP O_2), and a representative perivenous tension of 5% O_2 (PV O_2). The medium compositions were Std medium, (−) WRN, and (+) WRN. The (−) WRN medium was a 1:1 (v/v) mixture of Std medium and conditioned medium collected from L cells. The (+) WRN medium was a 1:1 (v/v) mixture of Std medium and conditioned medium collected from L-WRN cells. The L cells are a mouse mucosal cell line. The L-WRN cells are L cells engineered to constitutively express and secrete human WRN.

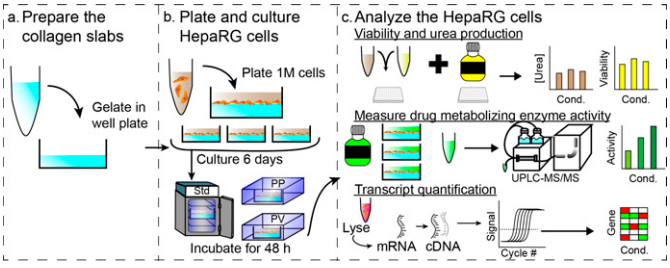

Fig. 1. Experimental workflow comparing the impact of oxygen tension and Wnt/β-catenin signaling on the expression and activity of drug-metabolizing enzymes in HepaRG cells. (A) First, 12-well plates were coated with collagen I (2 mg/ml). (B) Next, 1 × 10^6 cryopreserved HepaRG cells were seeded directly onto the collagen slab and incubated for 6 days under Std tissue culture conditions. The cells were placed in one of nine experimental conditions, combinations of three oxygen tensions and three culture medium compositions. (C) Lastly, the cells were evaluated for viability, urea production, and the activity and expression of drug-metabolizing enzymes.

In each experiment, the differentiated HepaRG cells were plated on collagen slabs and maintained at Std O_2 and in Std medium for 6 days before a 48-hour exposure to one of the nine experimental conditions. The timing of these experiments was determined empirically by tracking cell morphology and P450 activity for 24 days after plating. The cells transitioned from an undifferentiated spherical shape to a cobblestone-like pattern on Day 6 (Supplemental Fig. 2). This pattern persisted until Day 20, with hepatocyte-like cells maintaining a cuboidal or polygonal shape and the biliary-like cells a squamous or almond-like shape. The basal activity of CYP1A2, -2B6, -2C19, and -3A4 increased monotonically until Day 11 and then decreased until Day 24 (Supplemental Fig. 3). CYP2D6 reached maximum activity on Day 7. Initial transcript profiles of the HepaRG cells suggested significantly less *CYP2D6* than freshly isolated hepatocytes (Aninat et al., 2006). However, we and others measured 2D6-mediated metabolism of dextromethorphan or bufuralol with mass spectrometry (Jackson et al., 2016; Kvist et al., 2018).

The Influence of Oxygen on Viability and Cellular Health. The health and function of the HepaRG cells were unaffected by the different culture conditions used in this study, maintaining at least 80% viability across all three oxygen tensions (Fig. 2A) and in the presence of the WRN signaling molecules (Supplemental Fig. 4). Figure 2B plots the luminescence values obtained from the CTG assay for cells maintained under the three oxygen tensions. These results suggest an oxygen-mediated change in glucose metabolism and energy storage, indicated by cells in the PP and PV O_2 tensions having significantly lower ATP reserves than those in Std O_2 conditions. A previous study found that HepaRG glucose consumption was unchanged between 25% and 5% O_2, but cells at 5% O_2 had a higher output of lactate (van Wenum et al., 2018). In vivo, the average concentration of ATP per cell decreases significantly from the PP to PV region of the sinusoid (Berndt et al., 2021).

Urea synthesis is an indicator of liver-specific function and cell health (Bolleyn et al., 2015). Figure 2C shows HepaRG cells in PV conditions produced significantly more urea (0.023 ± 0.002 mg/ml/h/10^6) than cells maintained at standard or PP O_2 tensions (0.016 ± 0.003 mg/ml/h/10^6). Although our results contrast in vivo observations, there is experimental precedence that supports our findings. Li showed that HepaRG spheroids produce significantly more urea (3.0 mg urea/ml/10^6 cells) than monolayers (0.13 mg urea/mL/10^6 cells) under ambient oxygen tensions (Li et al., 2019). This increase could arise from the increased cell–cell and cell–extracellular matrix interactions in spheroids but more likely arises from the presence of an oxygen gradient spanning the cell mass. Oxygen gradients and hypoxic cores are common in cancer spheroids greater than 400 mm in diameter (Hirschhaeuser et al., 2010; Riffle and Hegde, 2017), an unavoidable phenomenon due to diffusional limitations in these three-dimensional structures. In perfused rat liver slices, urea production decreased with decreasing oxygen tension (Kari et al., 1987). Although these results are in line with in vivo findings, follow-up studies found the extent of urea synthesis in liver slices is dependent on oxygenation and the nutrient supply (Comar et al., 2007). This work found that 90% of hepatocytes express the enzymes needed for urea synthesis; this pathway can be activated as needed, regardless of location in the lobule hepatocytes. Further characterization of the HepaRG cells conditions is needed to determine how urea synthesis is regulated under the culture conditions we used.

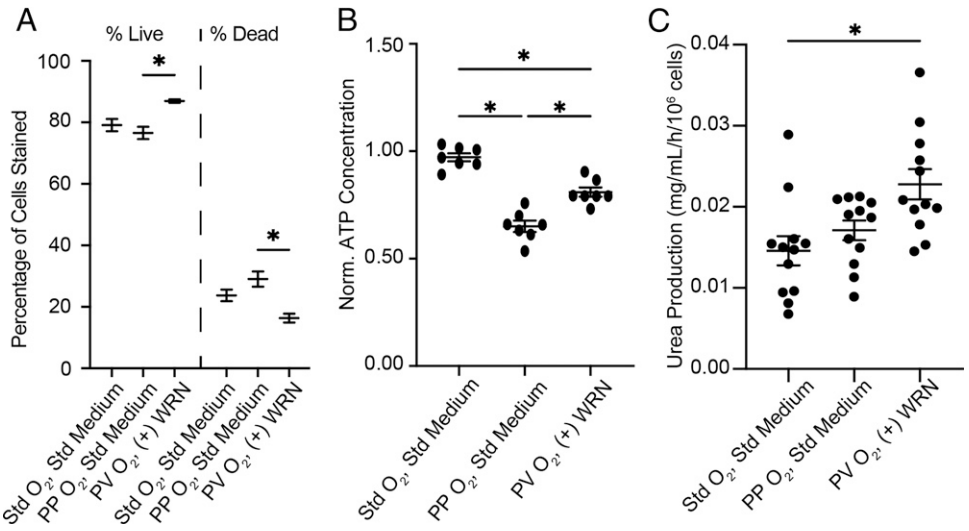

Fig. 2. Assessment of HepaRG viability, glucose, and health after a 48-hour exposure to the conditions denoted on the *x*-axis. (A) Viability was determined with calcein-AM (live cells), Hoechst 33343 (all cells), and propidium iodide (dead cells). Each data point represents the mean (line) and the range. (B) Glucose metabolism was indirectly measured with the CellTiter-Glo assay, which quantifies the ATP concentration in cell lysate. Each point represents a replicate culture, and the data are summarized with the mean (line) and S.E.M. (error bars). (C) Urea production was measured with a colorimetric assay. Each point represents a replicate culture, the data are summarized with the mean (line) and S.E.M. (error bars). All culture replicates were prepared from two vials of cryopreserved HepaRG cells. Significance (*P < 0.05) was determined with an ordinary two-way ANOVA with Tukey's multiple comparisons of the mean and variance.

O_2 Tension Influences on Enzyme Activity. Figure 3 compares the basal activity of drug-metabolizing enzymes in HepaRG cells maintained in Std medium and exposed to the Std O_2, PP O_2, or PV O_2 tension. The activity of CYP1A2, -2B6, and -3A4 decreased significantly at both physiologically relevant oxygen tensions. The activity of CYP2D6 and the UGT enzyme family also decreased significantly at the PP O_2 tension but returned to Std O_2 activity at the PV O_2 tension. The activity of the SULT enzymes increased with decreasing oxygen tension. Figure 3B replots this dataset for ease of comparison, focusing on changes in activity between the PP O_2 and PV O_2 tensions. This comparison highlights the significant increases in activity for all enzymes probed, except for CYP2C19. At PV O_2 tensions, the activity of CYP1A2 increased by 2.4-fold, -2D6 by 1.6-fold, -3A4 by 1.3-fold when probed with midazolam, and 1.5-fold when probed with testosterone. The SULT enzyme activity increased by 1.5-fold, and the UGT enzymes by 1.9-fold.

Wnt/β-Catenin Signaling Pathway Influences on Enzyme Activity. Figure 4 plots enzyme activity at each oxygen tension between the (−) WRN and (+) WRN medium conditions. Only CYP1A2 activity was significantly increased by the presence of the WRN molecules at all three oxygen tensions: a 2.3-fold increase at Std O_2, 2.9-fold increase at PP O_2, and 1.3-fold increase at PV O_2. CYP2B6 and -2C19 activities were unaffected by the WRN molecules at all three oxygen tensions. CYP2D6 activity significantly increased in the presence of the WRN molecules at PP O_2 tension (3.1-fold) but was unaffected at PV O_2 (1.1-fold). CYP3A4 activity increased at both Std O_2 and PP O_2 tensions in the presence of WRN: 1.9-fold when probed with midazolam and 2.0-fold when probed with testosterone at ambient oxygen; 2.2-fold when probed with midazolam and 1.5-fold when probed with testosterone at PP O_2 tensions. The SULT and UGT enzyme activities were only affected by the WRN molecules at PP O_2 tension, with a 1.4-fold decrease in SULT activity and a 1.7-fold increase in UGT activity. Additional comparisons of enzyme activity at each oxygen tension between the Std. medium, (−) WRN, and (+) WRN conditions is detailed in Supplemental Figs. 5 and 6.

Combined Effects of O_2 Tension and the Wnt/β-Catenin Pathway on Enzyme Activity. Figure 5 plots changes in enzyme activity at the PV O_2 tension in the absence or presence of the WRN signaling molecules, relative to activity at the PP O_2 tension in (−) WRN medium. These comparisons illustrate each factor's role in postdifferentiation patterning. The combination of oxygen and Wnt/β-catenin signaling significantly increased the activity of CYP1A1 (2.8-fold), -2D6 (2.3-fold), and -3A4 (2.3-fold when probed with midazolam and 2.4-fold when probed with testosterone). Oxygen tension accounted for at least two-thirds of the total activity increase in each instance. The UGT enzyme family activity increased 1.4-fold between the PP O_2 and PV O_2 conditions, but the addition of WRN had no significant effect (1.5-fold). Neither oxygen tension nor WRN molecules affected the activity of CYP2B6, -2C19, or the SULT family, suggesting these enzymes are regulated by another microenvironmental cue in the HepaRG cell line. A comprehensive comparison of enzyme activity in each medium condition, under PP and PV O_2 tensions, is included in Supplemental Fig. 7.

Transcriptional Changes between Standard Culture Conditions and PP and PV Microenvironments. Figure 6 highlights the transcription-level changes between the PP and PV O_2 tensions. In (−) WRN medium conditions, *CYP1A2* was significantly upregulated at the PV O_2 tension (6.7-fold). The expression of *CYP2C9*, *2C19*, and *2D6* decreased at the PV O_2 tension, whereas neither *CYP2B6* nor *-3A4* were affected. The additions of WRN signaling molecules, in both the PP and PV O_2, resulted in an increased expression of many *P450* transcripts. At the PP O_2 tension, the WRN molecules significantly increased the expression each of P450 probed, except for *CYP2D6* and *-3A4*. The increases were 2.6-fold for *-1A2*, 7.3-fold for *-2B6*, 10.6-fold for *-2C9*, 39.8-fold for *-2C19*, and 14.3-fold for *-2E1*. At the PV O_2 tension, the WRN molecules increased the expression of each P450 probed, except for *-2C9*. The increases at the PV O_2 tension were less than the PP O_2 but still significant. The increases were 3.6-fold for *-1A2*, 8.0-fold for *-2B6*, 2.2-fold for *-2C19*, 5.8-fold for *-2D6*, 3.5-fold for *-2E1*, and 8.6-fold for *-3A4*. The impact of the WRN molecules contrasts the activity data above, having a more significant effect on transcription than oxygen tension.

When compared with the PP O_2 tension, the combination of reduced oxygen tension and activated Wnt/β-catenin signaling increased the expression of each *P450* gene probed, except for *-2C9* and *-2C19*. Some of these increases were additive, whereas others like *-CY1A2* appear more synergistic. The increases were 23.7-fold for *-1A2*, 10.1-fold for *-2B6*, 2.60-fold for *-2D6*, and 11.4-fold for *-3A4*. These changes in P450 expression are difficult to correlate with the expression of the corresponding nuclear receptors, as neither oxygen nor the WRN molecules significantly changed the expression of *AhR*. Both *NR1I2* and *NR1I3* increased in the presence of the WRN molecules at the PP O_2 tension; this effect was not observed at the PV O_2 tension. Both *SULT2A1* and *UGT2B4* transcripts were downregulated in the PV O_2 tension, with and without WRN signaling molecules.

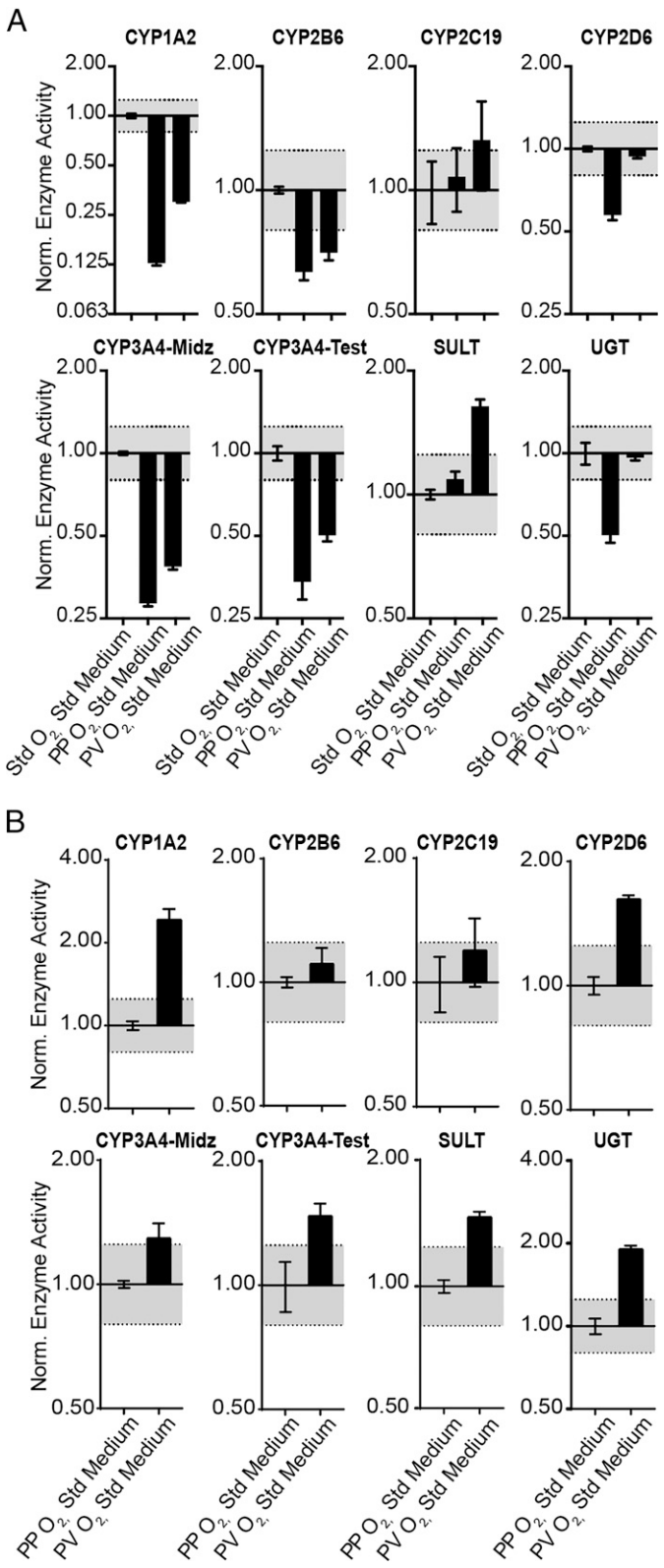

Fig. 3. Drug-metabolizing enzyme activity of HepaRG cells in 100% HepaRG medium (Std medium) after a 48-hour exposure to either Std, PP O_2, or PV O_2 tensions. (A) Enzyme activities in the PP O_2 and PV O_2 tensions, normalized to the activity at the Std O_2 tension. (B) Enzyme activities in the PV O_2 tension, normalized to the activity in the PP O_2 tension. The gray region on each graph represents non-significant changes in activity, the 99.99% deviation from repeated measurements of the same sample across multiple LC-MS/MS runs. Each bar represents the average and S.E.M. of at least four separate experimental setups, prepared from two vials of cryopreserved HepaRG cells.

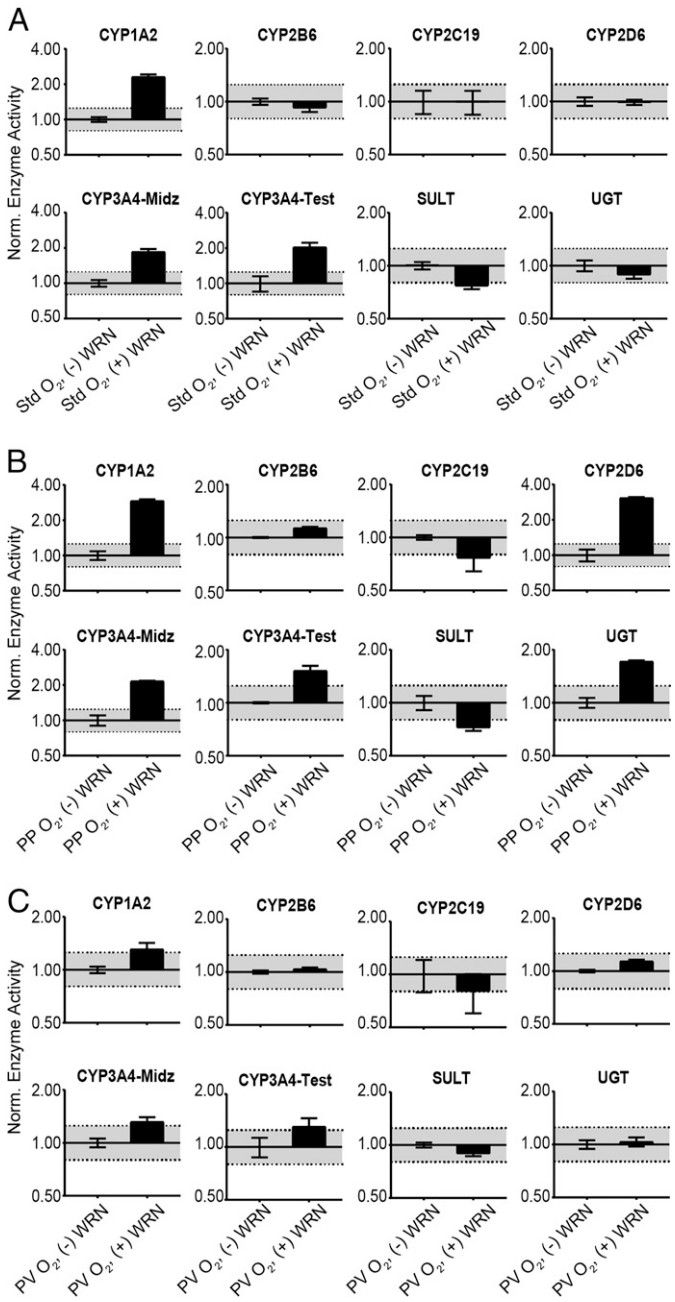

Fig. 4. Drug-metabolizing enzyme activity of HepaRG cells after a 48-hour exposure in a 1:1 (v/v) ratio of HepaRG medium and L-cell conditioned medium, (−) WRN; or a 1:1 (v/v) ratio of HepaRG medium and LWRN-cell conditioned medium, (+) WRN. Each dataset report enzyme activities at a single oxygen tension, normalized to the (−) WRN condition. The gray region on each graph represents nonsignificant changes in activity, the 99.99% deviation from repeated measurements of the same sample across multiple LC-MS/MS runs. Each bar represents the average and SEM of at least four separate experimental setups, prepared from two vials of cryopreserved HepaRG cells.

Discussion

Drug Metabolizing Enzyme Activity is Influenced by O_2 Tension. In vitro studies afford the experimental control over the cellular microenvironment needed to evaluate the role of individual components like O_2 tension without the risk of confounding variables, which are difficult to account for in vivo. Such studies determined that primary rat hepatocytes better maintain a differentiated state, high expression of *P450* transcripts, and liver-specific activity at physiologically relevant

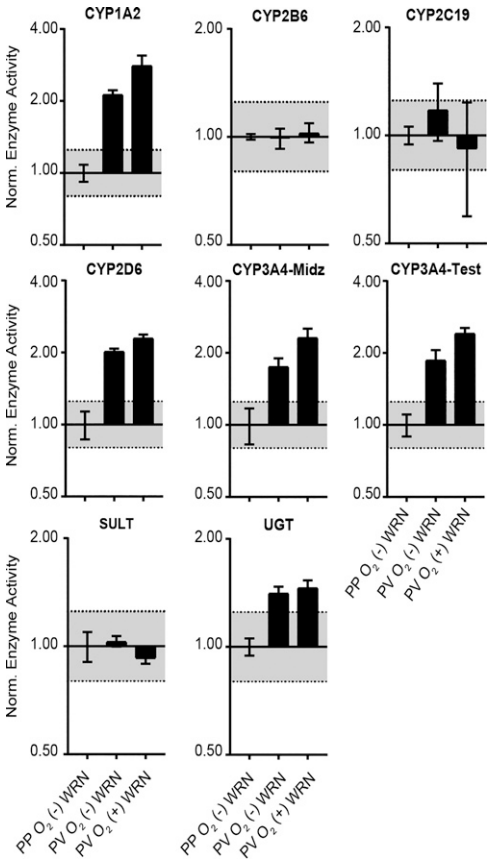

Fig. 5. Drug-metabolizing enzyme activity of HepaRG cells after a 48-hour exposure to PV O_2 tensions in (−) WRN and (+) WRN medium conditions, normalized to the enzyme activity at the PP O_2 tension in the (−) WRN conditions. The gray region on each graph represents nonsignificant changes in activity, the 99.99% deviation from repeated measurements of the same sample across multiple LC-MS/MS runs. Each bar represents the average and SEM of at least four separate experimental setups, prepared from two vials of cryopreserved HepaRG cells.

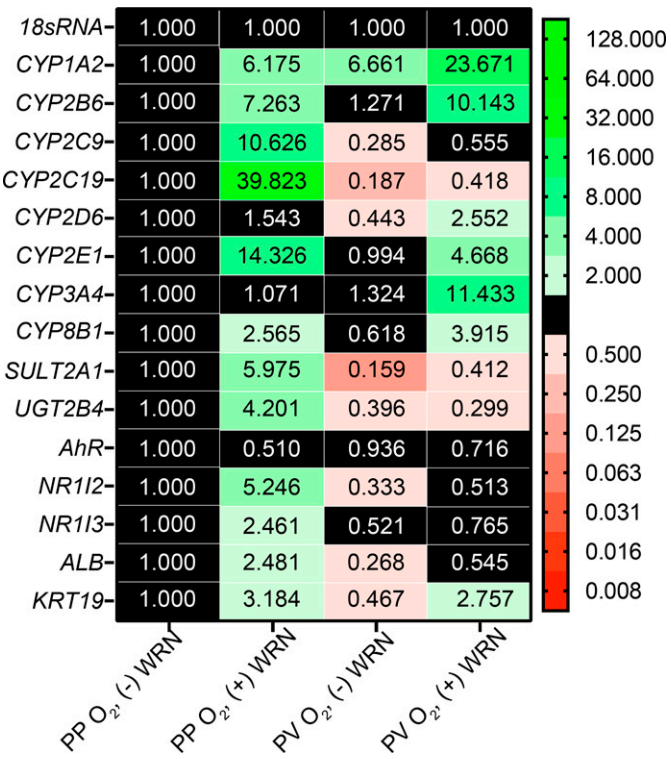

Fig. 6. Transcript-level regulation of drug-metabolizing enzymes and the associated nuclear receptors in HepaRG cells following a 48-hour exposure to PP O_2 or PV O_2 tensions. Fold-changes in expression, as determined with the ΔΔCt method, compared with cells in (−) WRN medium and exposed to Std O_2 tension. A fold change of ≥2.0 indicates a significant increase in expression and a fold change of ≤0.50 indicates a significant decrease. Each value is the average of at least two separate experimental setups, collected from two separate vials of cryopreserved HepaRG cells.

oxygen tensions (5% O_2) rather than the standard 20% O_2 (Guo et al., 2017). Legendre also showed HepaRG cells at 1% O_2 have significantly decreased CYP3A4, -1A2, -2E1, and -2C9 activity compared with standard culture conditions (Legendre et al., 2009). Hypoxia also decreased the expression of these *P450*s significantly, a process that was reversed after a 24-hour exposure to ambient oxygen tension.

We found physiologically relevant oxygen tensions differentially regulate the expression and activity of P450, SULT, and UGT enzymes. The significant decrease in CYP1A2, -2B6, -2D6, and -3A4 activity at physiologically relevant tensions is not surprising, given that most cells are selected in and maintained at standard culture conditions (Fig. 2A). This decreased activity was coupled with significant decrease in *P450* expression at both the PP O_2 and PV O_2 tensions (Supplemental Fig. 8). The activity of CYP2C19 was not affected by oxygen tension despite significant downregulation of its transcript at both PP O_2 and PV O_2 tensions. This unchanged activity cannot be attributed to an overall low basal activity, as -2C19 activity increased significantly 7 days after plating (2.5-fold) (Supplemental Fig. 2A). The metabolic product of -2C19 (4-hydroxymephenytoin) was easily distinguished from background.

Supplemental Figure 8 also shows the *AHR*, constitutive androstane receptor (CaR, *NR1I3*), and the pregnane X receptor (PXR, *NR1I2*) responsible for the transcription of the *P450* genes were also downregulated between standard and physiologic oxygen tensions. A similar oxygen-dependent decrease of these receptors was reported in a meta-analysis of prior work in primary hepatocytes (Zanger and Schwab, 2013). A recent study further confirmed the role of oxygen-related stress in the regulation of *P450*s (Takano et al., 2021). The introduction of selective inhibitors that stabilized HIF-α in primary human hepatocytes resulted in the downregulation of both *NR1I2* and *NR1I3*.

The comparison of enzyme activity under the PP O_2 and PV O_2 tensions (Fig. 3B) suggests the cells undergo postdifferentiation patterning. Specifically, CYP1A2, -2D6, and -3A4 activity increased significantly under PV O_2 tensions. The corresponding transcript changes (Supplemental Fig. 8B) support the activity data, with a 2.4-fold increase in *CYP1A2*, 5.3-fold for *CYP2D6*, and 4.6-fold increase for *CYP3A4*. Despite no change in either -2B6 or -2C19 activity (Fig. 3B), *-2B6* transcripts increased 7.2-fold and *-2C19* transcripts decreased 0.5-fold (Supplemental Fig. 8B). Transcriptional regulation of *AHR* agrees with the observed increase in both -1A2 expression and activity. A correlation between *NR1I2* and *NR1I3* and their corresponding *P450s* is less straightforward, as *NR1I2* is downregulated at PV O_2 tension and *NR1I3* is unchanged. Furthermore, there is known crosstalk between these receptors, which could contribute to the unexpected activity increases.

O_2 tension also altered the activity of the SULT and UGT enzyme families, further supporting hepatocyte postdifferentiation patterning. Compared with the PP O_2 tension, there was a significant increase in activity of both enzyme families at the PV O_2 tension (Fig. 3B). This increased SULT activity was unexpected given their localization in the PP region of the liver. The transcript data show significant upregulation

of *UGT2B4* but no change in *SULT2A1*, although direct comparisons are limited as single representative genes of each family.

The Presence of WRN Signaling Molecules Selectively Modulates P450 Activity at Each O_2Tension. Wnt and R-spondin ligands secreted by endothelial cells lining the central vein stabilize intracellular β-catenin in hepatocytes in the PV region of the liver, initiating the Wnt/β-catenin pathway (Rocha et al., 2015). Periportal hepatocytes express a negative regulator of β-catenin, adenomatous polyposis coli (Benhamouche et al., 2006). Sekine showed in the absence of β-catenin, PV hepatocytes in a Cre recombinase mouse model no longer expressed *CYP1A2* or *-2E1* (Sekine et al., 2006). They also showed that PP hepatocytes adopted a PV phenotype in the absence of adenomatous polyposis coli. In a separate study, Braeuning further demonstrated the role of β-catenin in both zonation and drug-metabolizing enzymes (Braeuning et al., 2009). In the absence of β-catenin, livers of their mice knockout model expressed significantly less *CYP1A2* and *-2C* family transcripts than the wild-type counterparts. The zonal distribution of *CYP1A2*, *-2B10*, *-2C* family, and *-3A* family transcripts was also less extreme in the absence of β-catenin.

In contrast to previous works, we used conditioned medium to activate the Wnt/β-catenin pathway. The experimental design corrected for other signaling molecules secreted by the L-WRN molecules by using conditioned medium from the parental L cells as a point of comparison. Although this approach has not been used in HepaRG or other hepatocyte-like studies, conditioned L-WRN medium is as effective as recombinant Wnt3a for the maintenance and differentiation of gastrointestinal stem cells (VanDussen et al., 2019). Wilson also found that the L-WRN conditioned medium outperformed medium containing each recombinant protein, maintaining and differentiating stem cell-generated organoids (Wilson et al., 2021). In particular, it resulted in enhanced activation of the Wnt/β-catenin pathway. This approach limits the overall resolution of a mechanistic study as the individual contributions of WRN is not discernible. Previous work by Thomas (Thomas et al., 2015), which focused on the addition of Wnt3a to HepaRG cells, agrees with our findings and suggests that conditioned medium, when appropriately corrected for, can reveal the effects of signaling pathway activation.

We found that cellular responses to Wnt/β-catenin pathway activation were O_2 tension-dependent. The WRN molecules significantly upregulated the expression of *CYP1A2*, *-2B6*, *-2C19*, -2D6, and *-3A4* (Supplemental Fig. 9) in the PV O_2 tension. These transcriptional changes resulted in a single significant change in enzyme activity: a 2.3-fold increase in -1A2 (Fig. 4C). At PP O_2 tensions (Fig. 4B), the WRN molecules significantly increased the activity of CYP1A2, -2D6, and -3A4. These increases agree with transcript data (Supplemental Fig. 9), which show the greatest response to the WRN molecules of the three oxygen tensions evaluated. Of the *P450* enzymes probed, only *-2D6* was not significantly upregulated by the addition of the WRN molecules at PP O_2. Thomas showed Wnt3a increased the expression of *CYP1A1* and *-2E1* but decreased the expression of *-2B6*, *-2C19*, and *-3A4* (Thomas et al., 2015). Our results comparing transcript levels of cells maintained at Std O_2 tension (Supplemental Fig. 8A show the (+) WRN medium increased *-2E1* expression, decreased *-2B6*, *-2C19*, and *-3A4* expression, and did not alter the expression of *-1A2*. In vivo, both Wnt/β-catenin signaling and P450 expression are elevated in PV regions of the sinusoid. Sekine showed that *CYP1A2* and *-2E1* expression was no longer detected in the livers of β-catenin knockout murine models (Sekine et al., 2006).

The SULT and UGT enzymes were also affected by the WRN molecules at the PP O_2 tension, suggesting they do have a role in the postdifferentiation of HepaRG cells. Although the expression of *SULT2A1* increased with the addition of the WRN molecules at the PP O_2, the overall activity of the SULT family decreased; both the expression of *UGT2B4* and activity of the UGT enzymes increased with the addition of the WRN molecules. These changes in SULT and UGT enzyme activity support a previous study by Giera (Giera et al., 2010), which showed Wnt/β-catenin regulates phase II enzyme zonation of the glutathione-S-transferase family of enzymes.

Direct comparisons of the PP and PV O_2 tensions in Fig. 5 best highlight postdifferentiation patterning of HepaRG, focusing on representative sinusoid microenvironments. The combination of the PV O_2 tension and WRN molecules significantly increased the activity of CYP1A2, -2D6, and -3A4. It also increased the activity of the UGT enzymes. For each of these increases, the decreased oxygen tension accounted for at least two-thirds of the total activity increase. For example, CYP1A2 activity increased 2.1-fold with the decreasing O_2 tension, but only an additional 0.7-fold when the WRN signaling molecules were added. These small increases in P450 activity caused by WRN molecules suggests that oxygen is the major contributor to postdifferentiation patterning in HepaRG cells.

The expression data for the PP and PV O_2 tensions (Fig. 6) indicate that the WRN molecules have a significant effect on the transcriptional regulation of drug-metabolizing enzymes. A comparison of cells exposed to the PP O_2 tension show a significant increase in expression for all genes probed, expect for *AhR*, *CYP2D6*, and *-3A4*, in the presence of the WRN molecules. The effects of the WRN molecules are further highlighted when comparing the PP O_2 (−) WRN condition with the PV O_2, (−) WRN, and PV O_2, (+) WRN conditions. As noted above, the decrease in oxygen upregulated only *CYP1A2* despite significance increases in enzyme activity. The addition of the WRN molecules increased the expression of *CYP1A2*, *-2B6*, *-2D6*, and *-3A4*; the expression of *CYP2C19*, *SULT2A1*, and *UGT2B4* also significantly decreased.

Conclusions

This study shows that HepaRG cells undergo postdifferentiation patterning when exposed to physiologically representative microenvironments. The experimental approach used in this study systematically evaluated the effects of both oxygen tension and Wnt/β-catenin signaling on the expression and activity of drug-metabolizing enzymes. These datasets complement previous studies and provide new insights into the role of these two environmental conditions, separately and in combination. Namely, oxygen tension is the primary regulator of P450 activity, whereas the Wnt/β-catenin pathway is the primary transcriptional regulator of *P450* expression. Discrepancies between P450 activity and expression highlight the need for thorough characterization of hepatocytes in basic and applied research endeavors, as transcript data alone may not give a complete picture of liver function. These results also highlight the importance of the cellular microenvironment in cell-based assays. This study focused on the basal metabolic activity of HepaRG cells but could just as easily be applied to studies predicting hepatotoxicity or potential drug–drug interactions. The postdifferentiation patterning of HepaRG induced by simple experimental changes further establishes this metabolically competent line as a resource in future drug metabolism studies and suggests the reevaluation of other hepatocyte-derived cell lines in nonstandard culture conditions.

Acknowledgments

The authors thank Dr. Brandie Ehrmann for her assistance with data analysis and instrument troubleshooting and Mr. Tyler Larson for helpful discussions as during manuscript preparation.

Authorship Contributions

Participated in research design: DiProspero, Lockett.

Conducted experiments: DiProspero, Brown, Fachko.

Performed data analysis: DiProspero, Lockett.

Wrote or contributed to the writing of the manuscript: DiProspero, Lockett.

References

Aninat C, Piton A, Glaise D, Le Charpentier T, Langouët S, Morel F, Guguen-Guillouzo C, and Guillouzo A (2006) Expression of cytochromes P450, conjugating enzymes and nuclear receptors in human hepatoma HepaRG cells. *Drug Metab Dispos* **34**:75–83.

Bell CC, Dankers ACA, Lauschke VM, Sison-Young R, Jenkins R, Rowe C, Goldring CE, Park K, Regan SL, Walker T, et al. (2018) Comparison of hepatic 2D sandwich cultures and 3D spheroids for long-term toxicity applications: a multicenter study. *Toxicol Sci* **162**:655–666.

Benhamouche S, Decaens T, Godard C, Chambrey R, Rickman DS, Moinard C, Vasseur-Cognet M, Kuo CJ, Kahn A, Perret C, et al. (2006) Apc tumor suppressor gene is the "zonation-keeper" of mouse liver. *Dev Cell* **10**:759–770.

Berndt N, Kolbe E, Gajowski R, Eckstein J, Ott F, Meierhofer D, Holzhütter HG, and Matz-Soja M (2021) Functional consequences of metabolic zonation in murine livers: insights for an old story. *Hepatology* **73**:795–810.

Bolleyn J, Rogiers V, and Vanhaecke T (2015) Functionality testing of primary hepatocytes in culture by measuring urea synthesis. *Methods Mol Biol* **1250**:317–321.

Braeuning A, Ittrich C, Köhle C, Hailfinger S, Bonin M, Buchmann A, and Schwarz M (2006) Differential gene expression in periportal and perivenous mouse hepatocytes. *FEBS J* **273**:5051–5061.

Braeuning A, Sanna R, Huelsken J, and Schwarz M (2009) Inducibility of drug-metabolizing enzymes by xenobiotics in mice with liver-specific knockout of Ctnnb1. *Drug Metab Dispos* **37**:1138–1145.

Comar JF, Suzuki-Kemmelmeier F, Nascimento EA, and Bracht A (2007) Flexibility of the hepatic zonation of carbon and nitrogen fluxes linked to lactate and pyruvate transformations in the presence of ammonia. *Am J Physiol Gastrointest Liver Physiol* **293**:G838–G849.

Dierks EA, Stams KR, Lim HK, Cornelius G, Zhang H, and Ball SE (2001) A method for the simultaneous evaluation of the activities of seven major human drug-metabolizing cytochrome P450s using an in vitro cocktail of probe substrates and fast gradient liquid chromatography tandem mass spectrometry. *Drug Metab Dispos* **29**:23–29.

DiProspero TJ, Dalrymple E, and Lockett MR (2021) Physiologically relevant oxygen tensions differentially regulate hepatotoxic responses in HepG2 cells. *Toxicol In Vitro* **74**:105156.

Dunn JC, Tompkins RG, and Yarmush ML (1992) Hepatocytes in collagen sandwich: evidence for transcriptional and translational regulation. *J Cell Biol* **116**:1043–1053.

Dunn JC, Yarmush ML, Koebe HG, and Tompkins RG (1989) Hepatocyte function and extracellular matrix geometry: long-term culture in a sandwich configuration. *FASEB J* **3**:174–177.

Gebhardt R, Baldysiak-Figiel A, Krügel V, Ueberham E, and Gaunitz F (2007) Hepatocellular expression of glutamine synthetase: an indicator of morphogen actions as master regulators of zonation in adult liver. *Prog Histochem Cytochem* **41**:201–266.

Gebhardt R and Matz-Soja M (2014) Liver zonation: Novel aspects of its regulation and its impact on homeostasis. *World J Gastroenterol* **20**:8491–8504.

Gerbal-Chaloin S, Dumé AS, Briolotti P, Klieber S, Raulet E, Duret C, Fabre JM, Ramos J, Maurel P, and Daujat-Chavanieu M (2014) The WNT/β-catenin pathway is a transcriptional regulator of CYP2E1, CYP1A2, and aryl hydrocarbon receptor gene expression in primary human hepatocytes. *Mol Pharmacol* **86**:624–634.

Gerets HH, Tilmant K, Gerin B, Chanteux H, Depelchin BO, Dhalluin S, and Atienzar FA (2012) Characterization of primary human hepatocytes, HepG2 cells, and HepaRG cells at the mRNA level and P450 activity in response to inducers and their predictivity for the detection of human hepatotoxins. *Cell Biol Toxicol* **28**:69–87.

Giera S, Braeuning A, Köhle C, Bursch W, Metzger U, Buchmann A, and Schwarz M (2010) Wnt/beta-catenin signaling activates and determines hepatic zonal expression of glutathione S-transferases in mouse liver. *Toxicol Sci* **115**:22–33.

Guo R, Xu X, Lu Y, and Xie X (2017) Physiological oxygen tension reduces hepatocyte dedifferentiation in in vitro culture. *Sci Rep* **7**:5923.

Hirschhaeuser F, Menne H, Dittfeld C, West J, Mueller-Klieser W, and Kunz-Schughart LA (2010) Multicellular tumor spheroids: an underestimated tool is catching up again. *J Biotechnol* **148**:3–15.

Jackson JP, Li L, Chamberlain ED, Wang H, and Ferguson SS (2016) Contextualizing hepatocyte functionality of cryopreserved HepaRG cell cultures. *Drug Metab Dispos* **44**:1463–1479.

Jungermann K and Kietzmann T (2000) Oxygen: modulator of metabolic zonation and disease of the liver. *Hepatology* **31**:255–260.

Kang YBA, Eo J, Bulutoglu B, Yarmush ML, and Usta OB (2020) Progressive hypoxia-on-a-chip: an in vitro oxygen gradient model for capturing the effects of hypoxia on primary hepatocytes in health and disease. *Biotechnol Bioeng* **117**:763–775.

Kari FW, Yoshihara H, and Thurman RG (1987) Urea synthesis from ammonia in periportal and pericentral regions of the liver lobule. Effect of oxygen. *Eur J Biochem* **163**:1–7.

Kenna JG and Uetrecht J (2018) Do in vitro assays predict drug candidate idiosyncratic drug-induced liver injury risk? *Drug Metab Dispos* **46**:1658–1669.

Kietzmann T (2017) Metabolic zonation of the liver: the oxygen gradient revisited. *Redox Biol* **11**:622–630.

Kietzmann T (2019) Liver zonation in health and disease: hypoxia and hypoxia-inducible transcription factors as concert masters. *Int J Mol Sci* **20**:2347.

Kvist AJ, Kanebratt KP, Walentinsson A, Palmgren H, O'Hara M, Björkbom A, Andersson LC, Ahlqvist M, and Andersson TB (2018) Critical differences in drug metabolic properties of human hepatic cellular models, including primary human hepatocytes, stem cell derived hepatocytes, and hepatoma cell lines. *Biochem Pharmacol* **155**:124–140.

Legendre C, Hori T, Loyer P, Aninat C, Ishida S, Glaise D, Lucas-Clerc C, Boudjema K, Guguen-Guillouzo C, Corlu A, et al. (2009) Drug-metabolising enzymes are down-regulated by hypoxia in differentiated human hepatoma HepaRG cells: HIF-1α involvement in CYP3A4 repression. *Eur J Cancer* **45**:2882–2892.

Li G, Huang K, Nikolic D, and van Breemen RB (2015) High-throughput cytochrome P450 cocktail inhibition assay for assessing drug-drug and drug-botanical interactions. *Drug Metab Dispos* **43**:1670–1678.

Li J, Settivari R, LeBaron M, and Marty M (2019) Functional comparison of HepaRG cells and primary human hepatocytes in sandwich and spheroid culture as repeated-exposure models for hepatotoxicity. *In Vitro Toxicol* **5**:187–195.

Matz-Soja M, Hovhannisyan A, and Gebhardt R (2013) Hedgehog signalling pathway in adult liver: a major new player in hepatocyte metabolism and zonation? *Med Hypotheses* **80**:589–594.

Meyer C, Liebe R, Breitkopf-Heinlein K, Liu Y, Müller A, Rakoczy P, Thomas M, Weng H, Bachmann A, Ebert M, et al. (2015) Hepatocyte fate upon TGF-β challenge is determined by the matrix environment. *Differentiation* **89**:105–116.

el Mouelhi M and Kauffman FC (1986) Sublobular distribution of transferases and hydrolases associated with glucuronide, sulfate and glutathione conjugation in human liver. *Hepatology* **6**:450–456.

Oinonen T and Lindros KO (1998) Zonation of hepatic cytochrome P-450 expression and regulation. *Biochem J* **329**:17–35.

Parasrampuria DA, Benet LZ, and Sharma A (2018) Why drugs fail in late stages of development: case study analyses from the last decade and recommendations. *AAPS J* **20**:46.

Riffle S and Hegde RS (2017) Modeling tumor cell adaptations to hypoxia in multicellular tumor spheroids. *J Exp Clin Cancer Res* **36**:102.

Rocha AS, Vidal V, Mertz M, Kendall TJ, Charlet A, Okamoto H, and Schedl A (2015) The angiocrine factor Rspondin3 is a key determinant of liver zonation. *Cell Rep* **13**:1757–1764.

Sekine S, Lan BY, Bedolli M, Feng S, and Hebrok M (2006) Liver-specific loss of beta-catenin blocks glutamine synthesis pathway activity and cytochrome p450 expression in mice. *Hepatology* **43**:817–825.

Shin DS, Seo H, Yang JY, Joo J, Im SH, Kim SS, Kim SK, and Bae MA (2018) Quantitative evaluation of cytochrome P450 3A4 inhibition and hepatotoxicity in HepaRG 3-D spheroids. *Int J Toxicol* **37**:393–403.

Takano H, Yamaguchi JI, Kato S, Hamada M, Tada M, and Endo H (2021) Downregulation of CYP1A2, CYP2B6, and CYP3A4 in human hepatocytes by prolyl hydroxylase domain 2 inhibitors via hypoxia-inducible factor-α stabilization. *Drug Metab Dispos* **49**:20–30.

Thomas M, Bayha C, Vetter S, Hofmann U, Schwarz M, Zanger UM, and Braeuning A (2015) Activating and inhibitory functions of WNT/β-catenin in the induction of cytochromes P450 by nuclear receptors in HepaRG cells. *Mol Pharmacol* **87**:1013–1020.

Center for Drug Evaluation and Research (2020) In vitro drug interaction studies – cytochrome P450 enzyme- and transporter-mediated drug interactions guidance for industry. U.S. Food and Drug Administration, Silver Spring, MD.

Usta OB, McCarty WJ, Bale S, Hegde M, Jindal R, Bhushan A, Golberg I, and Yarmush ML (2015) Microengineered cell and tissue systems for drug screening and toxicology applications: evolution of *in-vitro* liver technologies. *Technology (Singap World Sci)* **3**:1–26.

van Wenum M, Adam AAA, van der Mark VA, Chang JC, Wildenberg ME, Hendriks EJ, Jongejan A, Moerland PD, van Gulik TM, Oude Elferink RP, et al. (2018) Oxygen drives hepatocyte differentiation and phenotype stability in liver cell lines. *J Cell Commun Signal* **12**:575–588.

VanDussen KL, Sonnek NM, and Stappenbeck TS (2019) L-WRN conditioned medium for gastrointestinal epithelial stem cell culture shows replicable batch-to-batch activity levels across multiple research teams. *Stem Cell Res (Amst)* **37**:101430.

Wild SL, Elghajiji A, Grimaldos Rodriguez C, Weston SD, Burke ZD, and Tosh D (2020) The canonical Wnt pathway as a key regulator in liver development, differentiation and homeostatic renewal. *Genes (Basel)* **11**:1163.

Wilson SS, Mayo M, Melim T, Knight H, Patnaude L, Wu X, Phillips L, Westmoreland S, Dunstan R, Fiebiger E, et al. (2021) Optimized culture conditions for improved growth and functional differentiation of mouse and human colon organoids. *Front Immunol* **11**:547102.

Yokoyama Y, Sasaki Y, Terasaki N, Kawataki T, Takekawa K, Iwase Y, Shimizu T, Sanoh S, and Ohta S (2018) Comparison of drug metabolism and its related hepatotoxic effects in HepaRG, cryopreserved human hepatocytes, and HepG2 cell cultures. *Biol Pharm Bull* **41**:722–732.

Zanger UM and Schwab M (2013) Cytochrome P450 enzymes in drug metabolism: regulation of gene expression, enzyme activities, and impact of genetic variation. *Pharmacol Ther* **138**:103–141.

Address correspondence to: Matthew Ryen Lockett, University of North Carolina at Chapel Hill, Department of Chemistry, Kenan and Caudill Laboratories CB3290, Chapel Hill, NC 27599-3290. E-mail: mlockett@unc.edu

Drug Metabolism and Disposition
DMD-AR-2022-000870

Supporting Information for:

HepaRG cells adopt zonal-like drug-metabolizing phenotypes under physiologically relevant oxygen tensions and Wnt/β-catenin signaling

Thomas J. Diprospero [a], Lauren G.Brown [a], Trevor D. Fachko [a],
and Matthew R. Lockett [a,b]*

[a] Department of Chemistry, University of North Carolina at Chapel Hill, Kenan and Caudill Laboratories, Chapel Hill, North Carolina 27599-3290, United States

[b] Lineberger Comprehensive Cancer Center, School of Medicine, University of North Carolina at Chapel Hill, Chapel Hill, North Carolina 27599-7295, United States

* mlockett@unc.edu

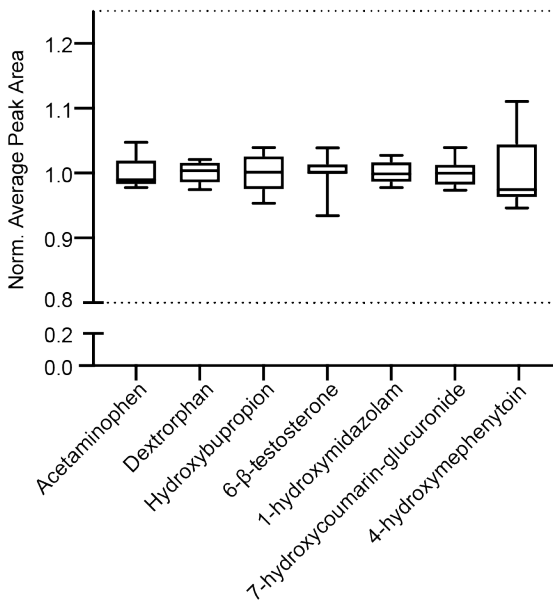

Supp. Fig. 1. Variability of repeated injections of a mixture of the eight products of CYP and the UGT enzymatic reactions, as determined with the LC-MS/MS method described in the Materials and Methods section. The mixture contained 10 μM of each product, dissolved in Optima water. In this box-and-whisker plot, the whiskers are the range; the upper box is the 75th percentile; the lower box is the 25th percentile; and the line represents the median measurement. The dashed lines represent four standard deviations of the mean, accounting for over 99.99% of deviation on a normal bell curve.

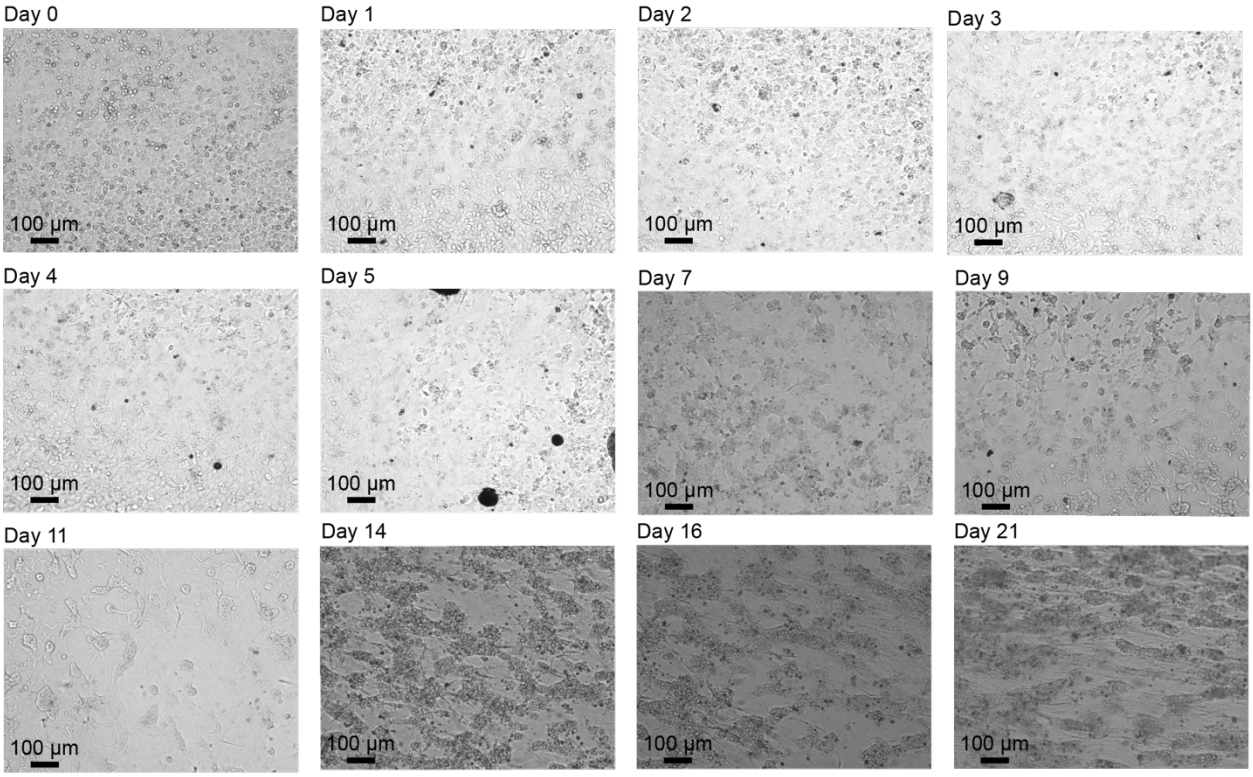

Supp. Fig. 2. Brightfield images of $1.0x10^6$ HepaRG cells plated on a 2 mg/mL collagen slab. Day 0 represents 4 h after plating, with cells having a uniform density across the surface of the slab and a rounded overall shape. On day 4, the a cobblestone morphology begins to form. On days 7 – 14, the cells maintain a cobblestone morphology and a cord-like network of islands of hepatocyte-like morphologies surrounded by cells with biliary-like morphologies. Each image was collected on a Nikon TE2000 microscope, equipped with a 10x Plan Fluor objective and a Photometrics Dyno CCD camera.

a.

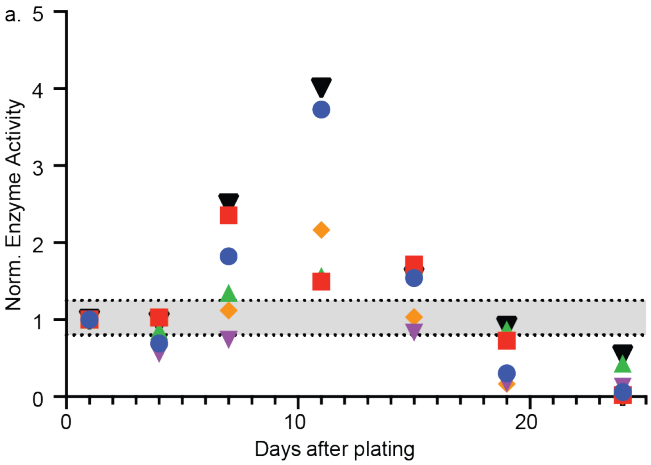

b.

	Day	Max. Activity (Fold-change)
CYP1A2	11	3.73
CYP2B6	15	1.70
CYP2D6	7	2.35
CYP2C19	11	4.01
CYP3A4-Midz	11	2.16
CYP3A4-Test	11	1.49

Supp. Fig. 3. CYP activity of 1.0×10^6 HepaRG cells on 2 mg/mL collagen slabs exposed to standard culture conditions for a 24-d period. Datasets at each time point represent a 2 h incubation in medium containing the six CYP substrates, normalized to the activity at Day 1. The grey region corresponds to non-significant changes in activity, and the 0.8- to 1.24-fold changes account for 99.99% deviation of repeated measurements across multiple LC-MS/MS runs.

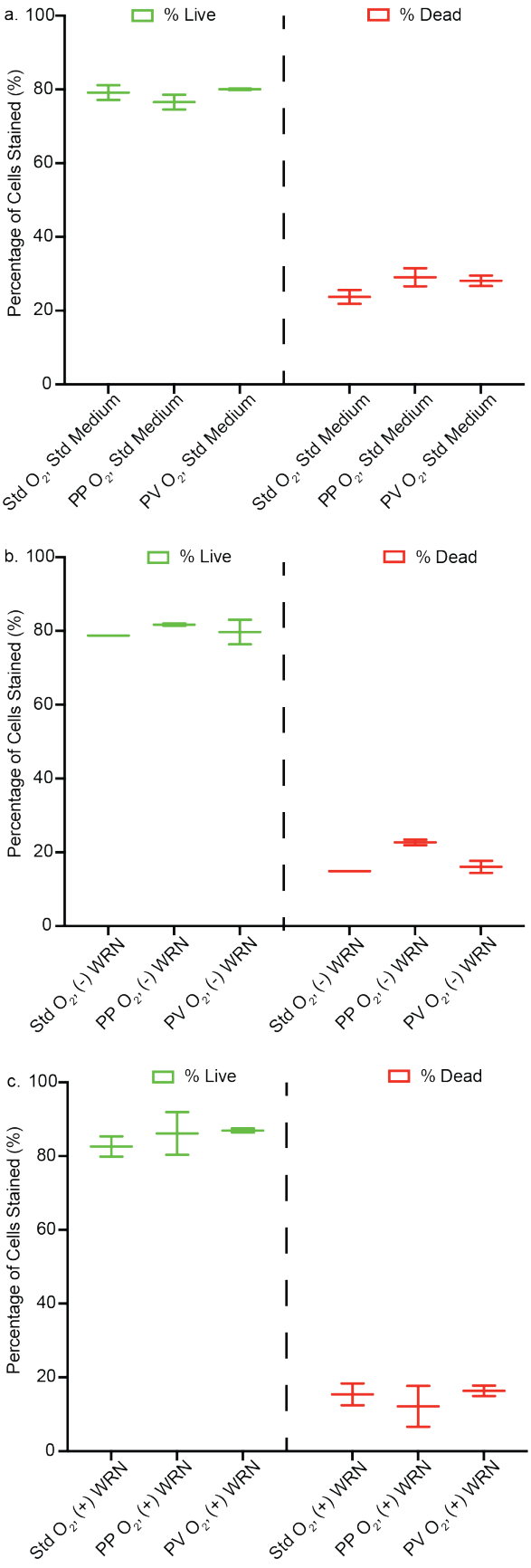
a.
% Live
% Dead
Percentage of Cells Stained (%)
0
20
40
60
80
100
Std O2, Std Medium
PP O2, Std Medium
PV O2, Std Medium
Std O2, Std Medium
PP O2, Std Medium
PV O2, Std Medium
b.
% Live
% Dead
Percentage of Cells Stained (%)
0
20
40
60
80
100
Std O2, (-) WRN
PP O2, (-) WRN
PV O2, (-) WRN
Std O2, (-) WRN
PP O2, (-) WRN
PV O2, (-) WRN
c.
% Live
% Dead
Percentage of Cells Stained (%)
0
20
40
60
80
100
Std O2, (+) WRN
PP O2, (+) WRN
PV O2, (+) WRN
Std O2, (+) WRN
PP O2, (+) WRN
PV O2, (+) WRN

Supp. Fig. 4. HepaRG viability after a 48-h exposure to Std, PP, or PV oxygen tension and a) HepaRG base medium, b) a 1:1 (v/v) mixture of HepaRG base medium and L-Cell conditioned medium, or c) a 1:1 (v/v) HepaRG base medium and L-WRN conditioned medium. Cell viability was determined with a tri-color stain, where live cells stained for both calcein-AM and Hoechst 33343 and dead cells stained for both propidium iodide and Hoechst 33343. Each datasets contains the mean and range of values from at least four separate cultures. Significance (*, $p < 0.05$) was determined with an ordinary two-way ANOVA with Tukey's multiple comparisons of the mean and variance.

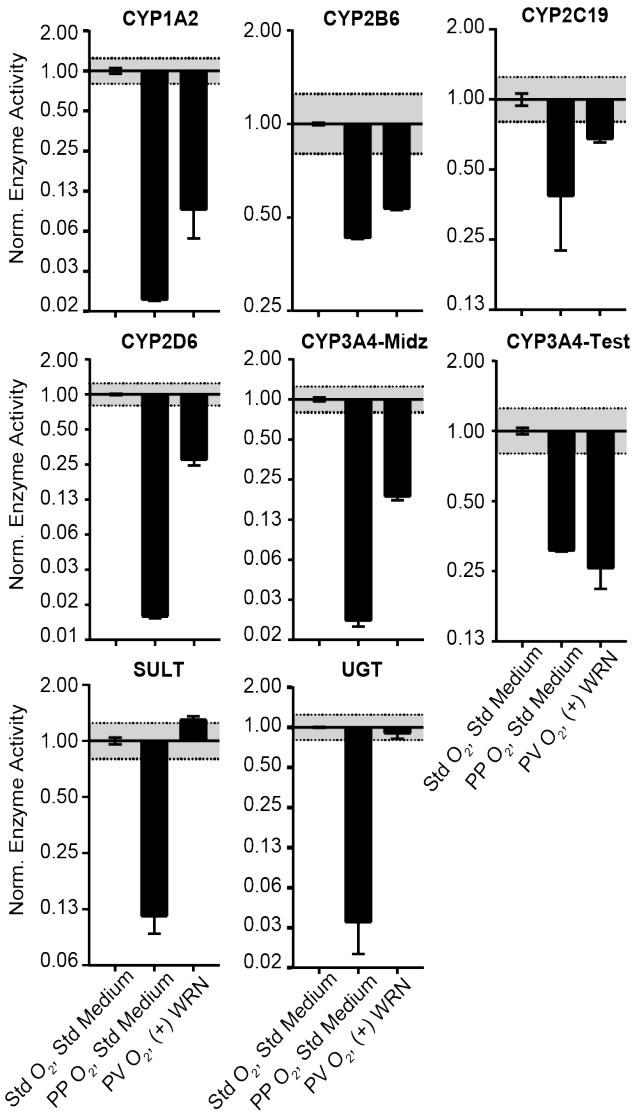

Supp. Fig. 5. Drug-metabolizing enzyme activity of HepaRG cells following a 48-h exposure to PP O_2 tension in standard culture medium or PV O_2 tension in (+) WRN medium, normalized to enzyme activity at standard culture conditions. The grey region on each graph represents non-significant changes in activity, the 99.99% deviation from repeated measurements of the same sample across multiple LC-MS/MS runs. Each bar represents the average and SEM of at least four separate experimental setups, prepared from two vials of cryopreserved HepaRG cells.

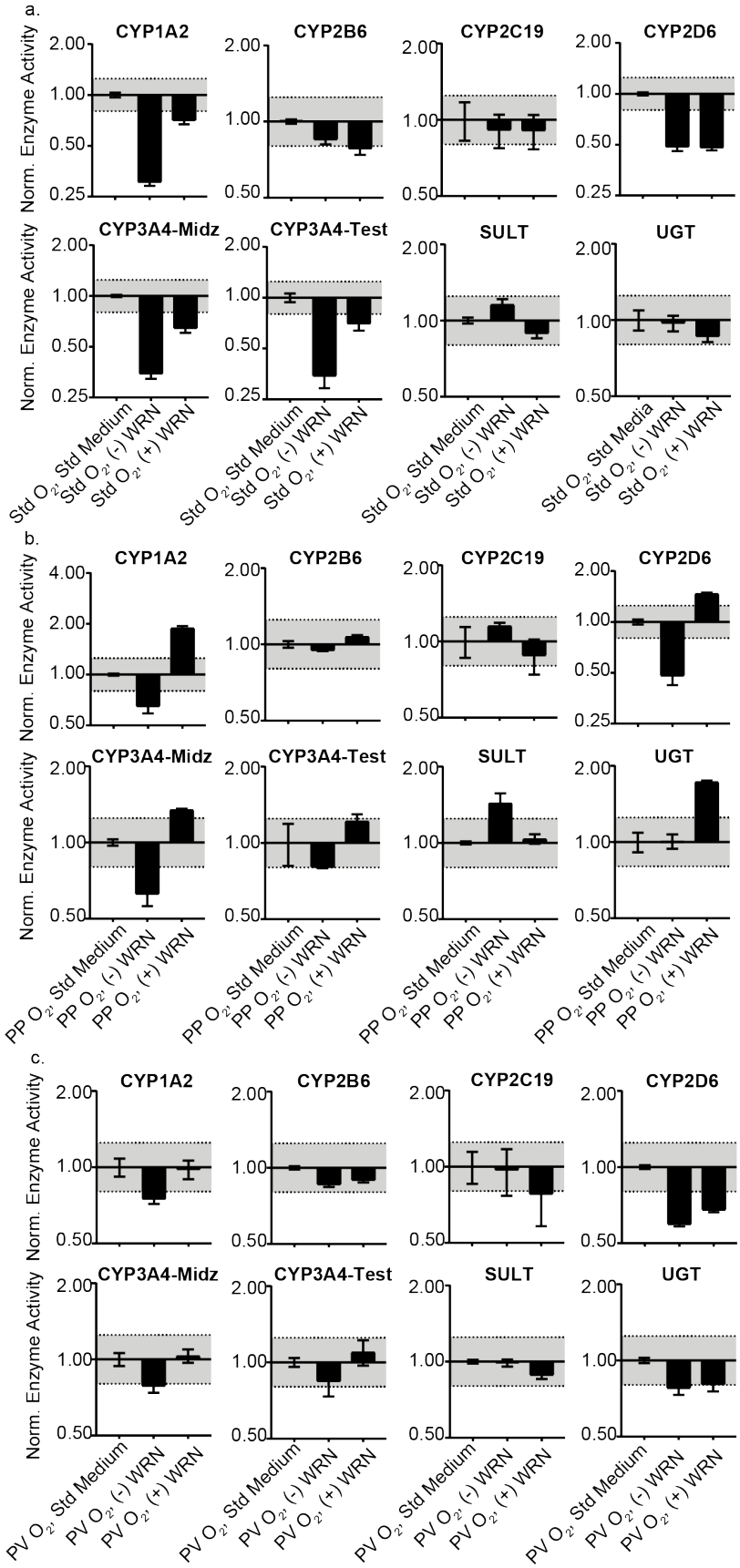
a.
CYP1A2
CYP2B6
CYP2C19
CYP2D6
CYP3A4-Midz
CYP3A4-Test
SULT
UGT
Norm. Enzyme Activity
Std O2 Std Medium
Std O2 (-) WRN
Std O2 (+) WRN
Std O2 Std Media
b.
PP O2 Std Medium
PP O2 (-) WRN
PP O2 (+) WRN
c.
PV O2 Std Medium
PV O2 (-) WRN
PV O2 (+) WRN

Supp. Fig. 6. Drug-metabolizing enzyme activity of HepaRG cells following a 48 h exposure to either Std, PP, or PV oxygen tensions. The cells were maintained in 100% HepaRG medium, Std Medium; a 1:1 (v/v) ratio of HepaRG medium and L-cell conditioned medium, (-) WRN; or a 1:1 (v/v) ratio of HepaRG medium and LWRN-cell conditioned medium, (+) WRN. Each dataset report enzyme activities at a single oxygen tension, normalized to Std Medium for a) Std O_2 tension, b) PP O_2 tension, or c) PV O_2 tension. The grey region on each graph represents non-significant changes in activity, the 99.99% deviation from repeated measurements of the same sample across multiple LC-MS/MS runs. Each bar represents the average and SEM of at least four separate experimental setups, prepared from two vials of cryopreserved HepaRG cells.

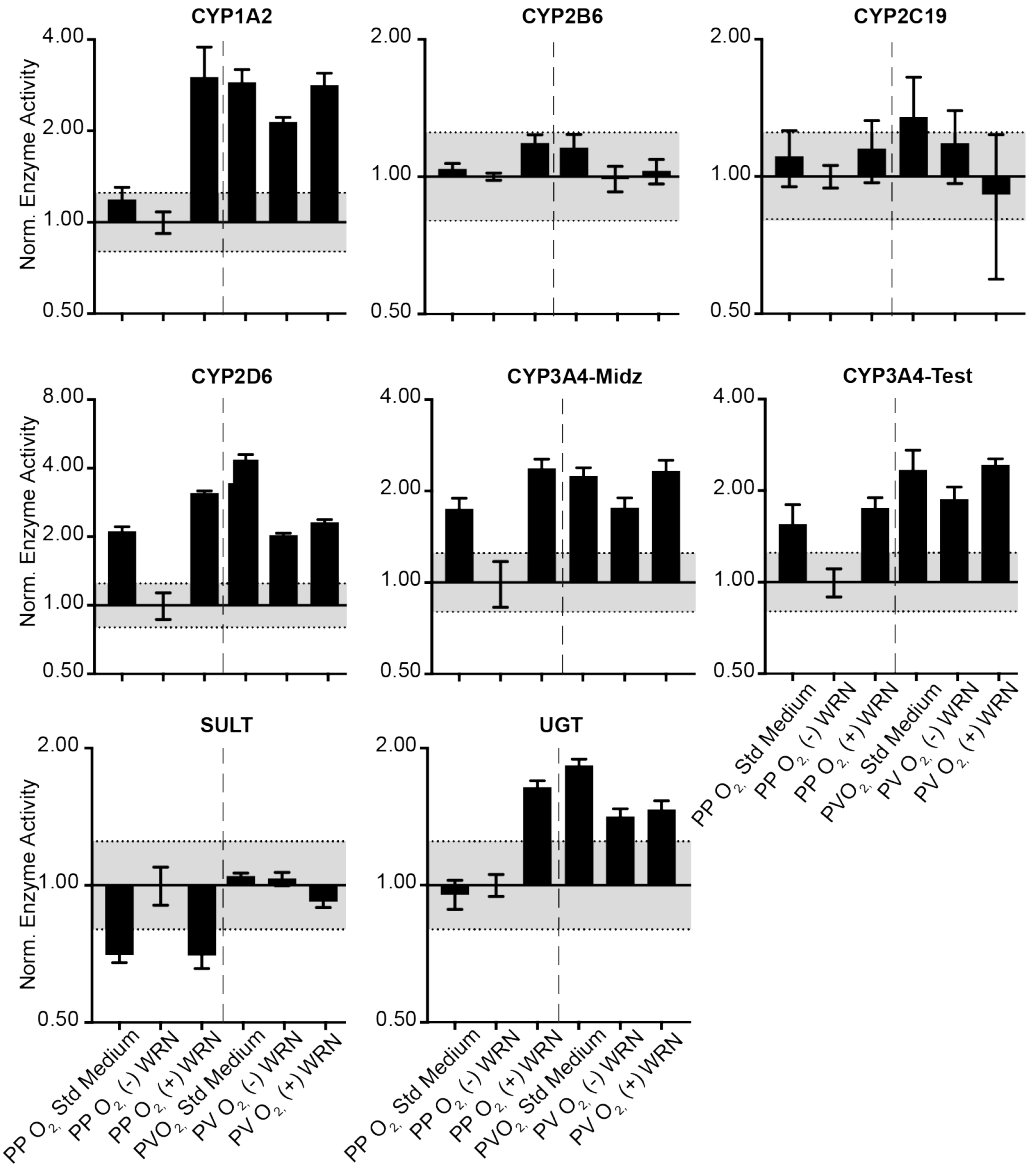

Supp. Fig. 7. Drug-metabolizing enzyme activity of HepaRG cells following a 48-h exposure to either PP or PV oxygen tensions, normalized to enzyme activity of cells in PP O2 tension and Std medium. The grey region on each graph represents non-significant changes in activity, the 99.99% deviation from repeated measurements of the same sample across multiple LC-MS/MS runs. Each bar represents the average and SEM of at least four separate experimental setups, prepared from two vials of cryopreserved HepaRG cells.

a.

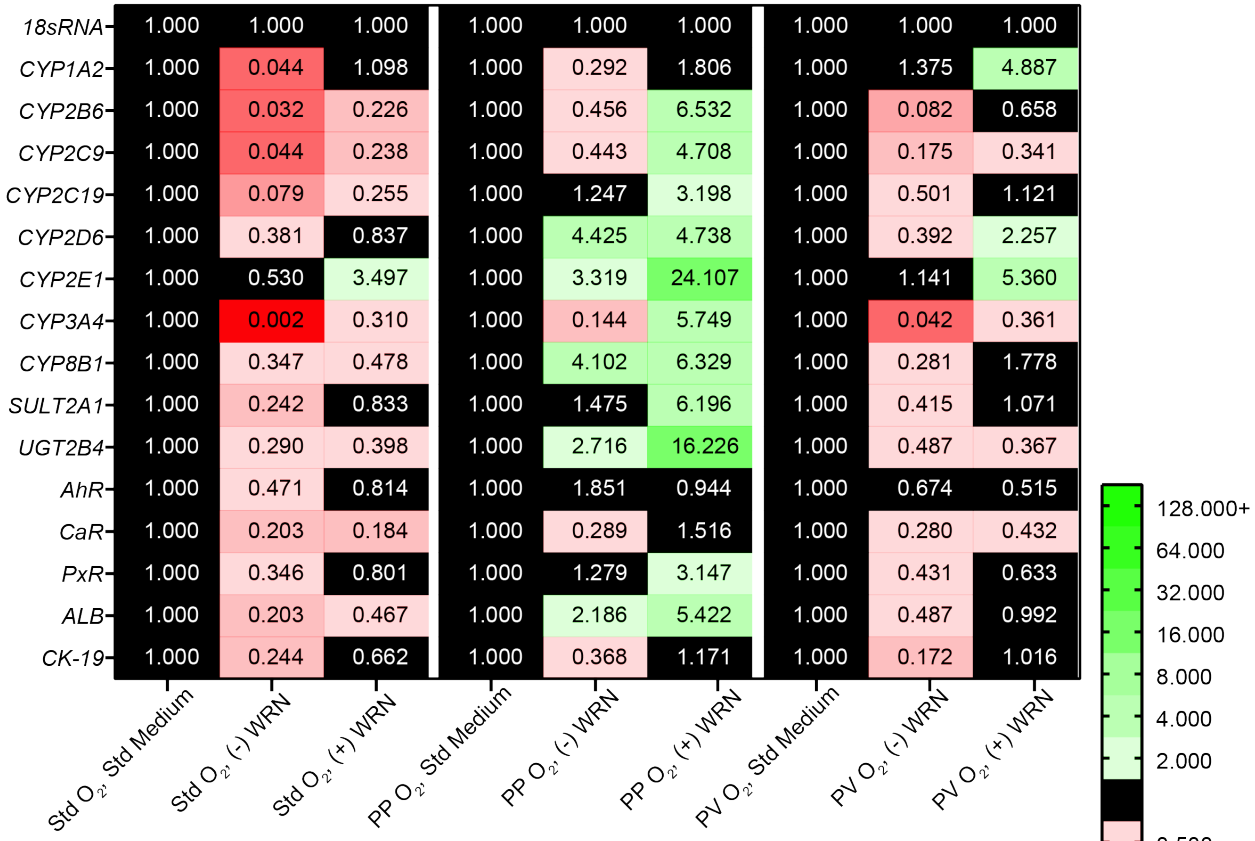
18sRNA 1.000 1.000 1.000 1.000 1.000 1.000 1.000 1.000 1.000
CYP1A2 1.000 0.044 1.098 1.000 0.292 1.806 1.000 1.375 4.887
CYP2B6 1.000 0.032 0.226 1.000 0.456 6.532 1.000 0.082 0.658
CYP2C9 1.000 0.044 0.238 1.000 0.443 4.708 1.000 0.175 0.341
CYP2C19 1.000 0.079 0.255 1.000 1.247 3.198 1.000 0.501 1.121
CYP2D6 1.000 0.381 0.837 1.000 4.425 4.738 1.000 0.392 2.257
CYP2E1 1.000 0.530 3.497 1.000 3.319 24.107 1.000 1.141 5.360
CYP3A4 1.000 0.002 0.310 1.000 0.144 5.749 1.000 0.042 0.361
CYP8B1 1.000 0.347 0.478 1.000 4.102 6.329 1.000 0.281 1.778
SULT2A1 1.000 0.242 0.833 1.000 1.475 6.196 1.000 0.415 1.071
UGT2B4 1.000 0.290 0.398 1.000 2.716 16.226 1.000 0.487 0.367
AhR 1.000 0.471 0.814 1.000 1.851 0.944 1.000 0.674 0.515
CaR 1.000 0.203 0.184 1.000 0.289 1.516 1.000 0.280 0.432
PxR 1.000 0.346 0.801 1.000 1.279 3.147 1.000 0.431 0.633
ALB 1.000 0.203 0.467 1.000 2.186 5.422 1.000 0.487 0.992
CK-19 1.000 0.244 0.662 1.000 0.368 1.171 1.000 0.172 1.016
Std O2, Std Medium
Std O2, (-) WRN
Std O2, (+) WRN
PP O2, Std Medium
PP O2, (-) WRN
PP O2, (+) WRN
PV O2, Std Medium
PV O2, (-) WRN
PV O2, (+) WRN
128.000+
64.000
32.000
16.000
8.000
4.000
2.000
0.500
0.250
0.125
0.063
0.031
0.016
0.008

b.

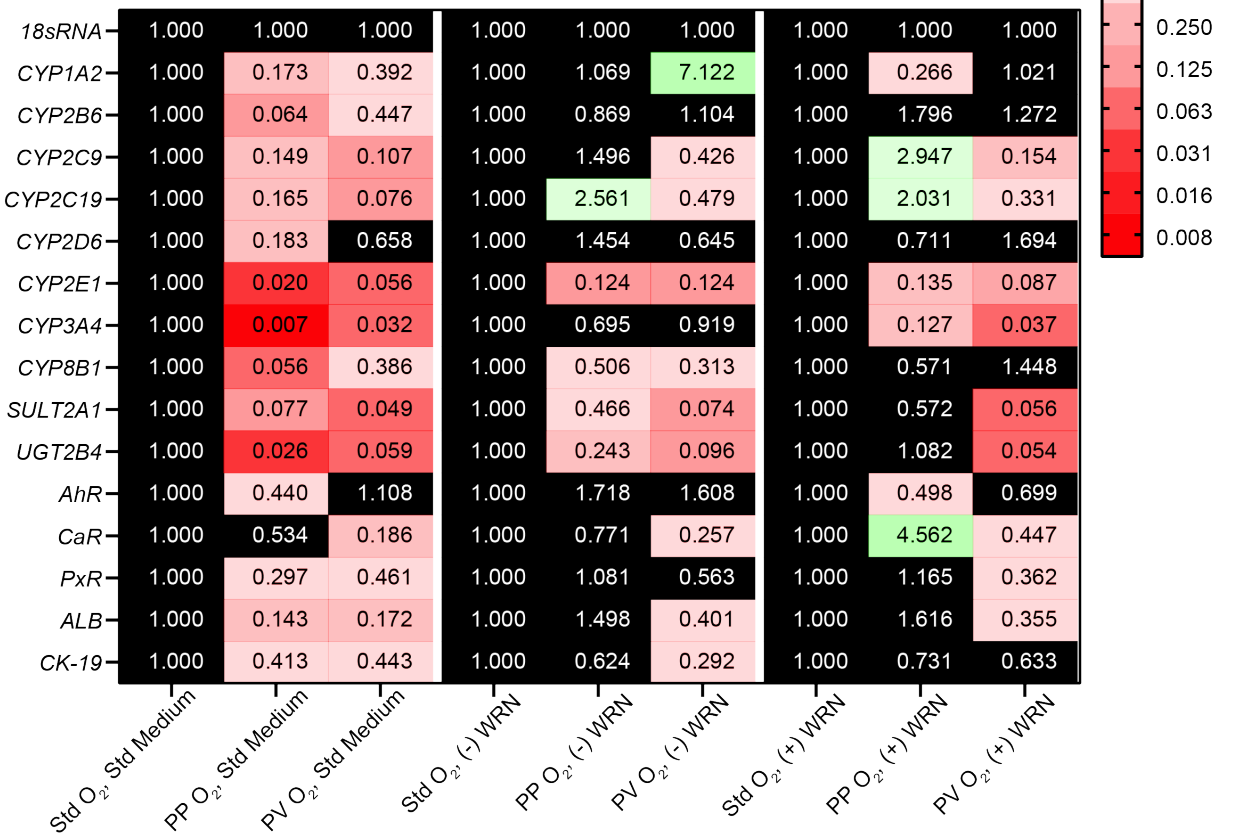
18sRNA 1.000 1.000 1.000 1.000 1.000 1.000 1.000 1.000 1.000
CYP1A2 1.000 0.173 0.392 1.000 1.069 7.122 1.000 0.266 1.021
CYP2B6 1.000 0.064 0.447 1.000 0.869 1.104 1.000 1.796 1.272
CYP2C9 1.000 0.149 0.107 1.000 1.496 0.426 1.000 2.947 0.154
CYP2C19 1.000 0.165 0.076 1.000 2.561 0.479 1.000 2.031 0.331
CYP2D6 1.000 0.183 0.658 1.000 1.454 0.645 1.000 0.711 1.694
CYP2E1 1.000 0.020 0.056 1.000 0.124 0.124 1.000 0.135 0.087
CYP3A4 1.000 0.007 0.032 1.000 0.695 0.919 1.000 0.127 0.037
CYP8B1 1.000 0.056 0.386 1.000 0.506 0.313 1.000 0.571 1.448
SULT2A1 1.000 0.077 0.049 1.000 0.466 0.074 1.000 0.572 0.056
UGT2B4 1.000 0.026 0.059 1.000 0.243 0.096 1.000 1.082 0.054
AhR 1.000 0.440 1.108 1.000 1.718 1.608 1.000 0.498 0.699
CaR 1.000 0.534 0.186 1.000 0.771 0.257 1.000 4.562 0.447
PxR 1.000 0.297 0.461 1.000 1.081 0.563 1.000 1.165 0.362
ALB 1.000 0.143 0.172 1.000 1.498 0.401 1.000 1.616 0.355
CK-19 1.000 0.413 0.443 1.000 0.624 0.292 1.000 0.731 0.633
Std O2, Std Medium
PP O2, Std Medium
PV O2, Std Medium
Std O2, (-) WRN
PP O2, (-) WRN
PV O2, (-) WRN
Std O2, (+) WRN
PP O2, (+) WRN
PV O2, (+) WRN

Supp. Fig. 8. Transcript-level regulation of drug-metabolizing enzymes and the associated nuclear receptors in HepaRG cells following a 48-h exposure to each of the nine conditions tested in this work. a) Fold-changes in expression, as determined with the ΔΔCt method, compared to cells in Std medium exposed to the Std, PP and PV O_2 tensions. b) Fold-changes in expression, as determined with the ΔΔCt method, compared to cells in Std O_2 tensions across Std Medium, the absence, and presence of WRN molecules (- WRN, +WRN). A fold-change ≥ 2.0 indicates a significant increase in expression and a fold-change ≤ 0.50 indicates a significant decrease. Each value is the average of at least two separate experimental setups, collected from two separate vials of cryopreserved HepaRG cells.

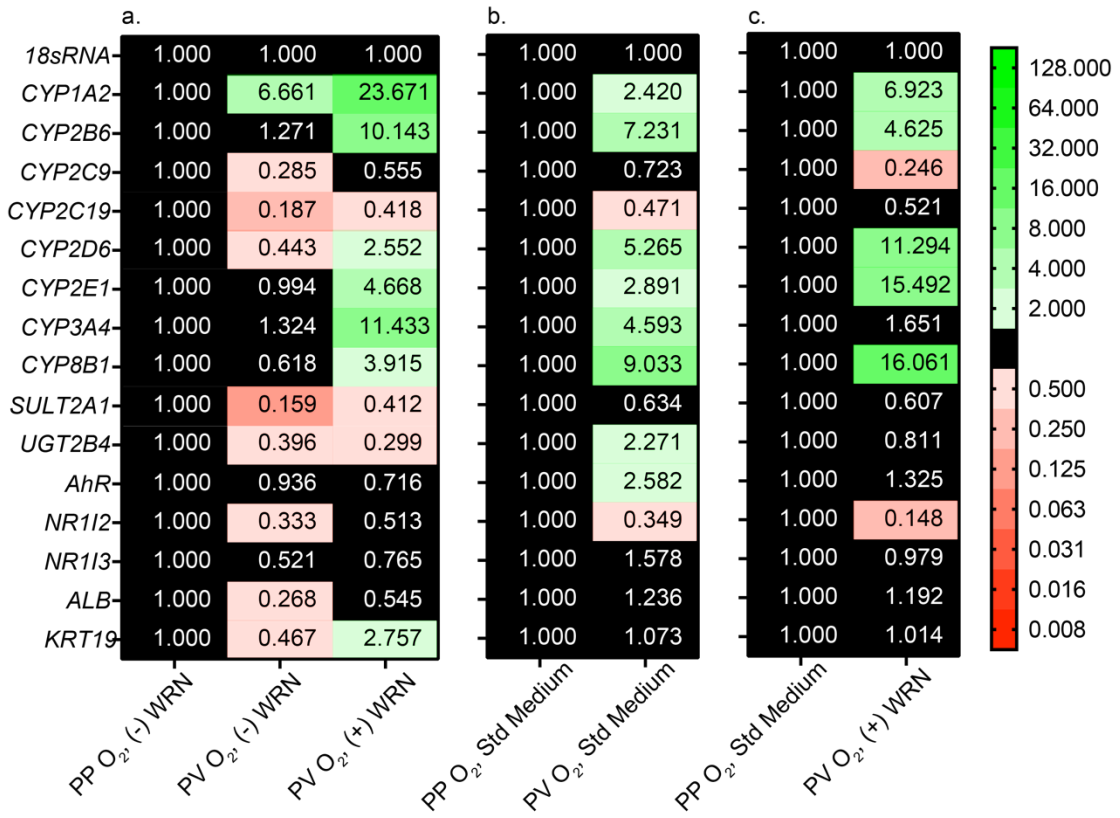

Supp. Fig. 9. Transcript-level regulation of drug-metabolizing enzymes and the associated nuclear receptors in HepaRG cells following a 48-h exposure to PP or PV O_2 tensions in the absence or presence of WRN molecules (- WRN, + WRN).a) Fold-changes in expression, as determined with the ΔΔCt method, compared to cells in PP O2 and the absence of WRN molecules. b) Fold-changes in expression, as determined with the ΔΔCt method, compared to cells in PP O_2 tensions and Std Medium. c) Fold-changes in expression, as determined with the ΔΔCt method, compared to cells in PP O_2 tensions and Std Medium. A fold-change ≥ 2.0 indicates a significant increase in expression and a fold-change ≤ 0.50 indicates a significant decrease. Each value is the average of at least two separate experimental setups, collected from two separate vials of cryopreserved HepaRG cells.

Supp. Table 1. MS/MS transitions monitored for each drug metabolizing enzyme

Enzyme	Substrate	Final concentration (μM)	Product/Isotope standard	Declustering voltage (V)	Ion mode	Parent ion (m/z)	Product ion (m/z)	Collision energy (eV)
CYP1A2	Phenacetin	100	Acetaminophen	6	Positive	152.2	110.0	15
						152.2	65.0	30
CYP2B6	Bupropion	50	Hydroxybupropion	6	Positive	256.0	238.1	8
						256.0	130.1	47
CYP2C19	(*S*)-mephenytoin	100	4-hydroxymephenytoin	6	Negative	232.9	190.1	19
						232.9	161.0	25
CYP2D6	Dextromethorphan	100	Dextrorphan	4	Positive	258.0	157.1	36
						258.0	199.1	25
CYP3A4	Midazolam	5	1-hydroxymidazolam	6	Positive	342.0	324.1	19
						342.0	168.1	36
CYP3A4	Testosterone	50	6-β-testosterone	8	Positive	305.2	269.2	13
						305.2	105.1	36
SULT	7-hydroxycoumarin	100	7-hydroxycoumarin sulfate	6	Negative	240.7	161.0	20
						240.7	133.0	34
UGT	7-hydroxycoumarin	100	7-hydroxycoumarin glucuronide	6	Negative	337.0	161.0	29
						337.0	175.0	13
CYP1A2			Acetaminophen-d_4	5	Positive	152.2	110.0	15
						152.2	65.0	30
CYP2B6			Hydroxybupropion-d_6	6	Positive	262.0	244.1	12
						262.0	130.0	43
CYP2C19			4'-hydroxymephenytoin-d_3	6	Negative	236.0	193.1	17
CYP2D6			Dextrorphan-d_3	4	Positive	261.2	157.1	40
						261.2	199.1	25
CYP3A4			1-hydroxymidazolam-[$^{13}C_3$]	10	Positive	345.1	327.1	18
						345.1	171.1	36
CYP3A4			6-β-testosterone-d_7	5	Positive	312.2	276.2	19
						312.2	294.1	11
SULT			7-hydroxycoumarin sulfate-d_5	0	Negative	245.1	165.0	31
						245.1	137.1	39

UGT	7-hydroxycoumarin-$^{13}C_6$-glucuronide	16	Negative	342.9	167.1	32
				342.9	139.1	29

Supp. Table 2. Transcripts evaluated with RT-qPCR

Gene symbol	Protein abbreviation	Main function	Forward primer (5' – 3')	Reverse primer (5' – 3')	Reaction efficiency (%)
18sRNA	18s rRNA	Ribosome	CGCCGCTAGAGGTGAAATTC	TTGGCAAATGCTTTCGCTC	107.5
CYP1A2	CYP1A2	Phase I Enzyme	CTTCGGACAGCACTTCCCTG	AGGGTTAGGCAGGTAGCGAA	103.9
CYP2B6	CYP2B6	Phase I Enzyme	TTCCTACTGCTTCCGTCTATC	GTGCAGAATCCCACAGCTCA	101.4
CYP2C9	CYP2C9	Phase I Enzyme	TCCCTGACTTCTGTGCTACATG	ACTGGAGTGGTGTCAAGGTTC	113.9
CYP2C19	CYP2C19	Phase I Enzyme	CAACAACCCTCGGGACTTTA	GTCTCTGTCCCAGCTCCAAG	106.2
CYP2D6	CYP2D6	Phase I Enzyme	ACCAGGCTCACATGCCCTA	TTCGATGTCACGGGATGTCAT	103.7
CYP2E1	CYP2E1	Phase I Enzyme	TTGAAGCCTCTCGTTGACCC	CGTGGTGGGATACAGCCAA	109.9
CYP3A4	CYP3A4	Phase I Enzyme	TCACAAACCGGAGGCCTTTT	TGGTGAAGGTTGGAGACAGC	100.4
CYP8B1	CYP8B1	Phase I Enzyme	TGCACATGGACCCTGACATC	GTGTCAGGGTCCACCAACTC	91.9
UGT2B4	UGT2B4	Phase II Enzyme	ACACATGAAGGCCAAGGGAG	GAACCAGGTGAGGTCGTGG	94.3
SULT2A1	SULT2A1	Phase II Enzyme	TGAGGAGCTGAAACAGGACAC	AAGTCTTCAGCTTGGGCCAC	106.6
AHR	AhR	Transcription Factor	CTTCCAAGCGGCATAGAGAC	AGTTATCCTGGCCTCCGTTT	101.5
NR1I3	CaR	Transcription Factor	TGATCAGCTGCAAGAGGAGA	AGGCCTAGCAACTTCGCATA	102.6
NR1I2	PxR	Transcription Factor	CCAGGACATACACCCCTTTG	CTACCTGTGATGCCGAACAA	104.3
ALB	Albumin	Globular Protein	TGAGCAGCTTGGAGAGTACA	GTTCAGGACCACGGATAGAT	124.1
KRT19	CK-19	Biliary-like/Progenitor Cell Marker	TTTGAGACGGAACAGGCTCT	AATCCACCTCCACACTGACC	100.8